Modeling Spatial Distributions of Tidal Marsh Blue Carbon using Morphometric Parameters from Lidar

Modeling Spatial Distributions of Tidal Marsh Blue Carbon using Morphometric Parameters from Lidar

A Thesis Presented

By

BONNIE TUREK

Submitted to the Graduate School of the
University of Massachusetts Amherst in partial fulfillment
of the requirements for the degree of

MASTER OF SCIENCE

February 2023

Department of Earth, Geographic, and Climate Sciences

Geography

Modeling Spatial Distributions of Tidal Marsh Blue Carbon
using Morphometric Parameters from Lidar

A Thesis Presented

By

BONNIE TUREK

Approved as to style and content by:

_____

Qian Yu, Chair

_____

Brian Yellen, Member

_____

Jonathan Woodruff, Member

_____

Piper R. Gaubatz, Department Head
Department of Earth, Geographic, and
Climate Sciences

ABSTRACT

MODELING SPATIAL DISTRIBUTIONS OF SALT MARSH BLUE CARBON USING MORPHOMETRIC PARAMETERS FROM LIDAR

FEBRUARY 2023

BONNIE TUREK, B.S., UNIVERSITY OF NEW HAMPSHIRE

M.S., UNIVERSITY OF MASSACHUSETTS AMHERST

Directed by: Professor Qian Yu

Tidal marshes serve as important "blue carbon" ecosystems that accrete large amounts of carbon with limited area. While much attention has been paid to the spatial variability of sedimentation within salt marshes, less work has been done to characterize spatial variability in marsh carbon density. Driven by tidal inundation, surface topography, and sediment supply, soil properties in marshes vary spatially with several parameters, including marsh platform elevation and proximity to the marsh edge and tidal creek network. We used lidar to extract these morphometric parameters from tidal marshes to map soil organic carbon (SOC) at the meter scale. Fixed volume soil samples were collected at four northeast U.S. tidal marshes with distinctive morphologies to aid in building our predictive models. Tidal creek networks were delineated from 1-m resolution topo-bathy lidar data using a semi-automated workflow in GIS. Sample distance to tidal creeks and flow distance to the marsh edge were then determined. Log-linear multivariate regression models were developed to predict soil organic content, bulk density, and carbon density as a function of these predictive metrics at each site and across sites. Results show that modeling salt marsh soil characteristics with morphometric inputs works best in marshes with simple, single creek morphologies. Distance from tidal creeks was the most significant model predictor. Addition of distance

to the inlet and tidal range as regional metrics significantly improves cross-site modeling. Our process-based approach results in predicted total marsh carbon stocks comparable to previous studies but provides trade-offs to existing simplistic carbon mapping methods. Further, we provide motivation to continue rigorous mapping of soil carbon at fine spatial resolutions and to use these results to guide salt marsh restoration projects and aid in the development of carbon markets.

TABLE OF CONTENTS

Page

LIST OF TABLES

LIST OF FIGURES

Figure Page

CHAPTER 1
INTRODUCTION

Tidal marshes, mangroves, and seagrass beds comprise what are known as "Blue Carbon Ecosystems" (BCEs), which refers to these systems' invaluable ability to store disproportionately large amounts of carbon within limited areas along the coast. Unlike upland ecosystems, which store much of their carbon in standing biomass, coastal wetlands sequester and store carbon mostly within their underlying sediments (Gulliver et al., 2020; McLeod et al. 2011). Predominantly saturated and anoxic soil conditions in tidal wetlands tend to preserve organic material in sediments for centuries to millennia, with sea level rise providing continual vertical accommodation space for additional soil carbon storage (Howarth & Hobbie, 1982; Morris et al., 2016). Globally, tidal marshes have been estimated to contain an average of 1-3 petagrams of near surface (biomass and top 1 meter of sediment) carbon stocks (Duarte et al., 2005; Duarte et al., 2013; Nahlik & Fennessy 2016; Pendleton et al., 2012). Marshes also have high primary productivity, serve as essential habitats for plants and animals (Barbier et al., 2011; Silliman & Bertness, 2002), provide protection along our coastlines from increasing impacts of flooding, erosion, and pollutants (Gedan et al., 2010; Shepard et al., 2011), and support recreational activities. Coastal development, land acquisition, sea level rise, and other environmental issues related to anthropogenic climate change pose threats to the integrity and extent of tidal marshes and their related carbon stocks (Deegan et al., 2012). These carbon stocks are also highly vulnerable to decomposition and potential re-emission of greenhouse gases into the atmosphere without proper management (Lovelock et al., 2017). An average salt marsh is thought to store 27 kgC/m^3 by volume in the United States (Holmquist et al., 2018), and based on global carbon stock estimates, a marsh

contains the equivalent of approximately 935 Mg CO_2/ha by area (Howard et al., 2014; IPCC, 2013). Loss of vegetated coastal ecosystems globally may contribute an additional 3–19% to recent estimates of global emissions from deforestation (Pendleton et al., 2012). While these may be large environmental concerns, quantifying tidal marsh blue carbon stocks for the development of "carbon markets" could create potentially large economic incentives to monitor and restore extant wetlands (Kroeger et al., 2017; Murray et al., 2011; Yang et al., 2020) and create new wetlands to sequester atmospheric carbon (IPCC 2019). However, large heterogeneity among studies and uncertainty regarding marsh soil carbon variability across various spatial scales impedes incentive structures that could facilitate blue carbon mapping projects. As blue carbon continues to accumulate interest and support in coastal research and policy-making, improvement in our ability to accurately measure rates of carbon accumulation and account for total carbon stocks is necessary (Hilmi et al., 2021).

Sediment organic carbon across a marsh is a function of bioproductivity, soil bulk density (BD), organic matter preservation, and mineral sediment content. The accumulation of sediment across a marsh is supported by two main mechanisms. These include the production and decomposition of organic matter by in situ vegetation and the delivery of allochthonous mineral and organic sediments via tidal inundation which become trapped by the vegetation (Bouillon et al., 2003; Mariotti et al., 2020; Saintilan et al., 2013; Temmerman et al., 2005). Relative sea level rise (RSLR) and marsh auto-compaction provide accommodation space for continuous sediment accretion and carbon storage (Allen, 2000). The competing natural processes of biomass production and decomposition in marshes ultimately dictate how much of the accumulating organic

sediment can be retained as carbon (Lalimi et al., 2018). Soil decomposition in marshes has been found to increase with increasing elevation and salinity, and decrease with increasing tidal inundation (Wang et al., 2019). Lowered water levels lead to increased oxygen availability in surface soils and can result in accelerated rates of organic matter decomposition (Laiho, 2006). Therefore, it is possible that increased tidal inundation may preserve soil carbon stocks via decreased decomposition. Vegetation structure and species composition, microbial community composition, temperature, and the physical and chemical soil conditions may also influence spatial patterns of biomass production and decomposition, and subsequently soil organic carbon (SOC) variability (Janousek et al., 2017; Kirwan et al., 2014; Valiela et al., 1985).

While much attention has been dedicated to the quantification of mineral sediment accretion rates in tidal marshes (e.g., Temmerman et al., 2003; van Proosdij et al., 2006), estimation of soil carbon variability in marsh peat is less understood (Chmura et al., 2003; Holmquist et al., 2018). Traditional methods for quantifying SOC in tidal marshes have been constrained by intensive, site-specific data collection, making it difficult to obtain reliable estimates of total blue carbon stocks at a broad regional scale. It is known that sedimentation varies widely and systematically at the marsh-scale, driven by tidal inundation magnitude and frequency, marsh surface topography, and sediment supply (Lalimi et al., 2018; Roner et al., 2016). Biomass production and decomposition rates also vary widely across marshes and across different sites (Marani et al., 2006; Morris et al., 2016; Nyman & Delaune,1991; Ursino et al., 2004). Therefore, it is thought that soil carbon may also be spatially dependent on several variables including marsh platform elevation, proximity to the marsh edge and tidal creek network, soil types, salinity

gradients, and vegetation percent cover and structure (IPCC, 2013; Kauffman et al., 2020; Roner et al., 2016; Temmerman et al., 2003).

Previous studies mainly estimate SOC in tidal wetlands based on existing categorical data and spatial interpolation. Holmquist et al. (2018) mapped carbon stocks in the continental U.S. (CONUS) based on existing soil, salinity and vegetation databases. Ultimately, Holmquist et al. (2018) found the best-performing strategy to be the assumption of a single empirical mean carbon density (CD) value. This resulted in a mean CD of 0.027 gC/cm^3 and an estimate of 0.72 petagrams (Pg) C within the top meter of CONUS tidal wetland soils (Holmquist et al., 2018). In regard to existing databases, U.S. Dept. of Agriculture Soil Survey Geographic (SSURGO) data were the best predictor of carbon density, where organic soils demonstrated higher CD than mineral soils. However, some features of existing national scale maps were misclassified, had missing or incomplete data, or did not overlap with mapped tidal wetlands, which led to errors and bias in carbon stock mapping as well. Holmquist et al. (2018) suggest future studies explore connecting the spatial variability of marsh soil carbon to ecologically and biogeochemically relevant processes rather than existing categorical maps. Twilley et al. (2018) examined global mangrove carbon storage as a function of morphological setting. Specific morphologies were assigned to each site based on the unique sedimentary and ecological processes in each as well as local hydrology, geomorphology, and climate. Mean carbon densities (to 1m depth) increased from river-dominated sites to tide and wave-dominated sites to carbonate coastlines. Based on mean CD for each of the morphological categories, the global mangrove SOC budget was estimated to be 2.3 PgC. Their results emphasize the role of environmental setting and geophysical controls in the

spatial diversity of coastal SOC stocks, which has potential to be even further refined when applied in different ecosystems and at a smaller scale. Kauffman et al. (2020) quantified ecosystem carbon stocks in seagrass beds, emergent marshes, and coniferous forested tidal wetlands along elevation and salinity gradients. Total carbon stocks increased with increasing elevation and decreasing salinity. Therefore, the lowest stocks were found in seagrass beds and highest stocks in forested tidal wetlands. Soil carbon also accounted for greater than 98% of total carbon stocks in the seagrass and marsh ecosystems. Their study suggests that sea-level rise and related effects such as increasing tidal inundation and pore water salinities could potentially decrease global soil carbon stocks in these ecosystems without proper management.

Several common predictive variables arise from these and other previous blue carbon studies, including surface elevation, tidal inundation and hydrological influences, salinity, site morphology, and soil characteristics for estimating total carbon stocks. While there has been more extensive documentation of C stocks in mangroves (e.g., Donato et al., 2011; Kauffman et al., 2014; Twilley et al., 2018), we seek to adapt previous findings and apply new techniques for mapping the spatial distribution of SOC in salt marshes. Temmerman et al. (2003) examined the integrated effects of some of these controlling variables on sediment delivery to the marsh platform. They used sediment traps to measure sedimentation as a function of position within the marsh. Temmerman's empirical method found that sedimentation rates strongly decreased with increasing surface elevation, increasing distance from the nearest tidal creek, and increasing creek distance from the marsh edge or outlet point. Previous studies estimated sedimentation and SOC patterns using conventional spatial interpolation methods such as kriging (van

Ardenne et al., 2018), which resulted in difficulties for interpolating between spatially-distributed measurements lacking constraints on associated uncertainties. In Temmerman's study, a single multiple regression model incorporating marsh elevation, tidal inundation above mean high water, and distance to tidal creeks and the marsh edge was used to successfully predict spatial patterns in marsh sedimentation.

By leveraging spatial metrics used by Temmerman et al. (2003) to predict spatial variability of sedimentation across a marsh, we propose using similar methods to model and map SOC at the meter scale using a process-based approach. Here we used lidar and tidal and geographic data to extract morphometric variables, including elevation, distance to tidal creeks, and distance to the marsh edge, as well as tidal range, tidal inundation, and marsh distance to the inlet, from four tidal marshes in the northeastern U.S. with varying morphologies. We analyzed spatial distribution of soil organic matter, dry bulk density, and soil carbon inventory as a function of these predictive metrics. Results from these sites will aid in building predictive models which can be compared and validated for implementation at a regional scale. Results from this study are expected to better inform resource managers of the quantity and variability of SOC in tidal marshes and provide essential guidance for estimating blue carbon storage and prioritizing marsh management at various spatial scales.

CHAPTER 2
METHODS

2.1 Site Description

We focused on four northeast US tidal marsh sites, including South River Marsh (Marshfield, MA), Westport River Marsh (Westport, MA), East River Marsh (Guilford, CT), and Hempstead Bay Marshes (Long Island, NY) (Figure 1). These sites were selected to capture a range of geomorphic and oceanographic settings (Table 1). South River Marsh (SR) is characteristic of a back-barrier estuarine system with a single connected creek network and is located approximately 4.5 km from the North and South Rivers inlet to Massachusetts Bay. East River Marsh in Guilford, Connecticut (ER) is an estuarine river system located directly at (<1 km) the mouth of the East River. Westport River Marsh (WP) is a partially-exposed fringing marsh within a larger embayment and located approximately 2.8 km from the estuary inlet. The Hempstead Bay marshes (HMP) are composed of several marsh islands within a back-barrier lagoon and located approximately 3.6 km from the inlet to the open ocean.

Tidal range varied from mesotidal at South River to microtidal at Westport River Marsh (Table 1). Each marsh site also has a unique mean high water (MHW) value based on local sea level, distance from the tidal river mouth and associated tidal attenuation. MHW for each site was determined as follows. We used a Hobo U20L pressure transducer to record continuous water levels within a marsh channel for at least two spring-neap cycles in 2018 at South River and 2019 at Westport River. Water levels were corrected for barometric pressure changes and salinity (See Yellen et al., in press). We used the NOAA Tidal Analysis Datums Calculator with the Boston gauge as a control station for South

River, and Newport, RI station as control for Westport River. At Hempstead and East River, we used historical NOAA field observations, which were available for each site. To account for sea level rise since the water level observations, we adjusted the MHW value for the observational period based on the amount of relative sea level rise since MHW observations were made. Therefore, MHW values for all sites are relative to the time and data analysis in 2022.

2.2 Sample Collection

We used marsh surface samples to characterize soil property spatial patterns for three primary reasons. First, we sought to quantify relationships between morphometric parameters and modern soil formation properties. Second, for the purpose of characterizing ongoing carbon sequestration, we were interested in capturing modern rates of carbon burial. Finally, by focusing on surface samples, which were quick to collect and process, we could maximize spatial coverage and better capture spatial variability than had we used 1 m cores. Ewers Lewis et al. (2020) used the same approach and rationale when mapping blue carbon variability in Australia. We collected samples from the top 10 cm of marsh soil, which based on regional average deposition rates represents approximately 21 years of accumulation based on 10 dated cores north of Cape Cod (South River site) (O'Keefe-Suttles, 2019) and 28 years of accumulation based on 14 dated cores at our other three sites south of Cape Cod (Hill and Anisfeld, 2015). We designed our sampling methodology to minimize compaction, thereby accurately capturing sediment bulk density, and to collect sufficiently large samples to capture centimeter-scale variability in field soil properties. This concept of the minimum sample

size that captures soil variability is taken from hydrology and is referred to as the representative elementary volume (Bear, 1972).

Surface samples were collected in transects at each marsh site in June and July of 2021. Generally, tidal marsh soil characteristics vary in relation to distance from major tidal creeks (e.g., Roner et al., 2016). Therefore, we established transects extending perpendicular from tidal creeks. Since the nature of northeast US tidal marshes include complex networks of meandering tidal channels of varying widths and extensive anthropogenic ditching, accessibility by foot was also considered in transect selection. Last, we collected a few limited transects of samples between ditches and parallel to tidal creeks to evaluate whether proximity to ditches influenced marsh soil properties. We collected surface samples with a 7.4 cm internal diameter aluminum core tube approximately 25 cm long. The corer was rotated while pushing down in order to cut through fibrous material and minimize compaction. We oversampled the surface material to a depth of approximately 15 cm, dug the sample out of the marsh, then extruded the core until exactly 10 cm of material remained, and sliced off the excess with a knife. Surface samples had a volume of 418 cm^3. Samples were placed into plastic sample bags and transported to the University of Massachusetts where they were stored at 4°C until ready for analysis. A total of 242 sediment samples were collected at all marsh sites, with 76 samples from South River, 93 samples from Westport, 27 samples from East River, and 44 samples from Hempstead Bay. We surveyed sampling locations to the NAVD88 vertical datum using a real time kinematic GPS (RTK) unit corrected in real time via statewide continuously operating reference networks. RTK unit self-reported horizontal

and vertical error was generally less than 3 cm, consistent with published values for this survey method (Aykut et al., 2015).

2.3 Sample Analysis

Surface samples were weighed wet and dry, then homogenized in a food processor and subsampled for loss on ignition (LOI) analysis following procedures described in Dean (1974). Samples were first dried and weighed to calculate dry bulk density in g/cm^3, defined as sample total dry mass divided by the fixed sample volume of 418 cm^3. Dry, homogenized sediment subsamples of approximately 20 cm^3 were then combusted in a muffle furnace at 550°C for 5 hours. The change in subsample mass was calculated after combustion to determine the organic mass from loss on ignition (LOI) analysis. To test whether our subsamples were representative of a 418 cm^3 sample, we used a sample splitter to divide a sample in half. We combusted one half, and measured LOI on ten subsamples from the other half. The half sample LOI was 42.5%. The mean of the subsamples was 42.1%, with a standard deviation of 1.5%. From this, we determined that measurements from subsamples were representative. Sample LOI was used as a proxy for soil organic matter (SOM). LOI was converted to total organic carbon (TOC) percentage following the conversion method from Ouyang and Lee (2020), which reported an R^2 = 0.99 (*P<.001)* fit between LOI and TOC for tidal marsh sediments. Percent organic carbon for each sample was converted to carbon density in gC/cm^3 as the product of total organic carbon and bulk density. Variation in measured sediment characteristics within each marsh site and across marsh sites are reported, with emphasis on differences between South River and Westport due to higher sample sizes and distinct morphologies.

2.4 Spatial Modeling of Soil Carbon

2.4.1 Individual-Site SOC Model

Digital elevation models (DEMs) at 1m spatial resolution derived from lidar were acquired for each of the tidal marsh sites from the online NOAA Digital Coast Data Viewer. We used a low tide lidar DEM for each study site (see Table 1) and selected between available datasets based on coverage, date, and year of data collection, horizontal and vertical accuracy, and resolution. For each site, the lidar DEM, sample coordinates, and their respective soil characteristics were loaded into ArcGIS Pro. Semi-automated tidal creek delineation was performed for each marsh site using the lidar datasets and GIS Hydrology tools. This process begins with running flow direction and flow accumulation tools. Then the proper threshold for flow accumulation was tested so as to create a stream network best matching the water channels shown on high resolution remote sensing images. We tested the soil property variability between ditches and parallel to major tidal creeks. Based on the observation that SOC did not vary systematically between ditches, we selected to include 3rd order and higher creeks in our creek network delineation, but not ditches, which were typically first and second order channels. At each soil sample location, we calculated the following morphometric parameters: the height of tidal inundation over the marsh above MHW (H), the Euclidean distance from the nearest tidal creek (Dc), and the shortest creek distance from the marsh outlet or the "marsh edge" (De). Variation in derived morphometric metrics across sampled marsh site sections are reported using one-way analysis of variance (ANOVA).

We analyzed patterns of measured marsh sediment characteristics with distance from tidal creeks along several transects at each site. Our analysis focused on differences between South River and Westport sites, which represent marsh morphological end members. A multivariate model based on three combined lidar-derived morphometric parameters was established to predict LOI, BD, and CD, following similar methods to those used in Temmerman et al. (2003) to predict sediment delivery to the marsh. The log-linear predictive model is presented here:

$$\log LOI = a(H) + b(Dc) + c(De) + k \quad \text{(eq.1)}$$

$$\log BD = a(H) + b(Dc) + c(De) + k \quad \text{(eq. 2)}$$

$$CD = BD*TOC = BD * (0.52 * LOI * 100 - 1.17)/100 \quad \text{(eq.3)}$$

Where:

LOI is the fractional loss-on-ignition (a proxy for SOM),

BD is dry bulk density in g/cm^3,

a, b, c are fitted model coefficients (separate values for eq. 1 and 2),

k is the model intercept (separate values for eq. 1 and 2),

H is local tidal inundation height over marsh platform elevation at MHW (MHW-z) in meters,

Dc is the sample distance from the nearest tidal creek in meters,

De is the creek distance from the marsh edge in meters, and

CD is carbon density in gC/cm^3, following the conversion between LOI and percent total organic carbon **(TOC)** from Ouyang and Lee (2020).

Equations 1 and 2 above describe the model form for relating LOI and BD to morphometric parameters at each site. Equation 3 describes the calculation of modeled

carbon density using the modeled BD, LOI, and the conversion from LOI to TOC described in Ouyang and Lee (2020).

Predictive spatial models were established using derived morphometric parameters, H, Dc, and De, for sampling locations at which we measured sediment characteristics. We used an ordinary least squares approach to fit model coefficients using the Scikit-learn machine learning Python package (Pedregosa et al., 2011). Implementing equations 1-3, best fit model coefficients k, a, b, and c, were determined to obtain predicted LOI, BD, and CD values for each sample. This resulted in two best fit model equations for each site: a best-fit LOI equation and a best fit BD equation (eight single-site model equations in total). All CD equations were based on results from LOI and BD models. This resulted in one CD model per site, and four unique CD models.

2.4.2 Cross-Site SOC Model

In order to test our method across multiple sites without fitting model parameters to individual sites, we created cross-site models for LOI, BD, and CD for all 242 sampling locations over four marsh sites in the northeastern U.S. The cross-site model derived parameters from Equations 1 and 2 to all of the observed morphometric parameters described above and in Temmerman et al., (2003). The Temmerman et al. (2003) sedimentation model was applied at only one marsh location, a fringing marsh within the Scheldt Estuary. Dc, De, and H are model metrics to determine the spatial variation of soil organic carbon within a marsh, however we are also interested in capturing spatial trends between marsh estuaries. Considering northeast marshes often exhibit a dominant sediment supply at the marine inlet (e.g., Baranes et al., 2022; Fitzgerald et al., 2020;

Geyer et al., 2001; Hopkinson et al., 2018), we incorporated distance from the estuarine inlet (Di) to our soil observation points and the model. We added a tidal range term (TR) to our model as well to examine spatial differences between marsh sites. The fully developed cross-site model is represented below.

$$\textit{log Parameter} = a(H) + b(Dc) + c(De) + d(Di) + f(TR) + k \quad \text{(eq.4)}$$

Where:

Parameter represents either LOI or BD to be modeled,

a, b, c, d, f are fitted model coefficients,

k is the model intercept,

Di is distance from the marsh edge to the inlet, and

TR is the marsh tidal range.

2.4.3 Grid-Based SOC Mapping

Based on the regression models, we generated maps of the two-dimensional spatial patterns of SOM, BD, and CD in a grid-based (raster) GIS. This was done for marsh sites that performed well with the morphometric models. For each grid cell that represents the marsh surface, a value of H, Dc and De was calculated. H can be calculated by taking the MHW value for each site and subtracting the marsh platform elevation values from the lidar (MHW-z). Therefore, H was derived for the entire marsh platform based on continuous lidar datasets. Dc was calculated by the Euclidean Distance tool from the tidal creek network. De is defined as the sum of the straight-line distance to the nearest creek (i.e., Dc) and downstream distance along the flow path to the marsh edge, called flow length (Figure 2). The flow length was first derived along all streams and creeks by the Flow Length tool in ArcGIS Pro and then each landscape grid cell was assigned the flow

length value of its nearest creek point using the Distance Allocation tool. Dc and flow length were finally summed using the raster calculator to derive De for each grid cell. SOM, BD, and CD values in every marsh surface cell were calculated by implementing Equations 1-3 and the calculated values of H, Dc and De.

CHAPTER 3
RESULTS

3.1 Intersite Soil Properties Comparison

Based on our measurements of LOI, BD, and CD from marsh surface samples, soil properties varied within and between marsh sites with different morphologies. (Figure 3; Table 2). East River had the lowest median LOI (0.19) and highest median BD (0.44 g/cm^3). Westport had the highest median LOI (0.50) and lowest median BD (0.17 g/cm^3). Based on a one-way ANOVA test, the median LOI of measured samples at Westport was significantly higher than median LOI at South River (WP, 0.50 > SR, 0.34; $P<.001$). Variation in BD across South River and Westport marshes was also statistically significant, with South River having a higher median BD (SR, 0.23 g/cm^3 > WP, 0.17 g/cm^3; $P<.001$). All other site pairings demonstrated statistically significant variation in median LOI and BD ($P<.001$), with the exception of Westport and Hempstead. These sites had very similar median LOI and BD (average LOI, 0.50; average BD, 0.175 g/cm^3). Measured CD variation between sites was smaller than that observed for LOI and BD (Figure 3). Mean as well as median observed CD was approximately 0.042 gC/cm^3 for all sites. However, Hempstead demonstrated the highest median CD of 0.047 gC/cm^3 and was statistically different from all other sites ($P<.001$).

3.2 Lidar-Derived Morphometric Parameters

Tidal inundation varied across each marsh and between marsh sites. This is largely influenced by local mean high water (MHW), as well as marsh platform elevation (Table 1). Variation in MHW and marsh platform elevation across the sites affected the model parameter H, or amount of tidal inundation above MHW across each marsh, therefore

influencing the results of the models. Our sample locations at the three southerly sites (WP, ER, and HMP), which all have lower tidal ranges, indicated average elevation above the level of MHW, resulting in negative inundation values (H) (Figure 4). At South River, our sampling location elevations were on average 0.12 m below MWH, reflecting positive H values, greater tidal inundation, and greater preponderance of low marsh at that site relative to our other sites. It is important to note that these comparisons reflect variation in derived morphometric parameters for the selected marsh section samples rather than the overall marsh complex at each site. Distance parameters Dc and De vary somewhat predictably, with lower values and smaller ranges at the fringing marsh at Westport and the island marshes at Hempstead. Conversely, Dc and De at our estuarine river sites, South River and East River, were higher and had larger ranges, likely due to the morphology of the marsh site section. South River and East River marsh sections exhibit a longer and more sinuous connected creek network versus Westport and Hempstead which have a higher density of shorter tidal creeks for the sections sampled.

3.3 Spatial Relationships

Sample data from marsh transects confirm spatial relationships between lidar-derived morphometric parameters and sediment characteristics. We present transect data from Westport and South River as representative sites from a multi-creek embayment site and single channel back-barrier marsh site, respectively (Figure 5). Transects from Hempstead and East River Marsh are presented in the supplementary material (Figure S1). Since soil properties did not vary systematically between first and second order ditches, our selected transects were oriented perpendicular to third order and higher creeks to determine spatial patterns with soil properties and Dc values. Measured LOI,

our proxy for SOM, generally increased with increasing distance from tidal creeks, Dc, and increasing distance from the marsh edge, De, (Figure 5). Measured bulk density values suggest opposite relationships, with bulk density inversely related to Dc and De. BD was typically highest within the first 20m of the creek bank, where mineral sediment is delivered via tidal creeks, then decreased significantly, leveling off approximately 20m from the creek bank. Spatial relationships with CD were less clear across sites, as carbon density is a function of organic content and soil bulk density, which demonstrate opposing spatial trends with morphometric parameters. Model prediction ability along these transects (gray lines, Figure 5) was generally better for South River transects than Westport transects. The model successfully predicted the increase of SOM along South River transects but was less successful in predicting exceptionally high BD at locations proximal to creeks (<20m). Largely, the models predicted BD to be fairly constant with Dc across all selected transects. The models also consistently underpredicted CD values.

3.4 Individual-Site Model Results

Success of predictive morphometric models varied by site. Each of the marsh sites has a unique set of model coefficients and R^2 and RMSE values for LOI, BD, and CD models (Figure 6; Table 3). South River and East River sites, which share similar morphologies, performed best with predicting spatial variability of all sediment characteristics. Specifically, the South River models were most successful in predicting LOI ($R^2 = 0.68$), and the East River models were most successful in predicting BD ($R^2 = 0.70$). The models for marsh sites with shorter and more numerous creeks, Westport and Hempstead, were less successful. R-squared values for LOI and BD models at Westport and Hempstead ranged from 0.08-0.16. Models from all sites demonstrated greater challenges

in predicting CD, a function of LOI and BD, resulting in R-squared values ranging from 0.01-0.25. South River models most successfully predicted CD ($R^2 = 0.25$).

As reflected in the shapes of relationships in Figure 6, almost all model-predicted LOI, BD, and CD ranges were smaller than measured ranges for each site. Predicted ranges of BD and resultant CD were particularly smaller, especially at Westport and Hempstead sites. For example, the measured range of BD at Westport was approximately 0.1-0.5 g/cm^3, while model predicted BD values only ranged from approximately 0.1-0.2 g/cm^3. At South River and East River sites, predicted LOI, BD, and CD ranges were more comparable to measured ranges.

Individual-site model coefficients a, b, and c, and their respective p-values presented in Table 3 reflect the relationship and relative influence each model parameter had on predicting spatial variability of sediment characteristics. Fitted values for coefficient 'a' in South River and East River LOI models were negative with significant p-values ($P<.001$), suggesting an inverse relationship between model parameter H and LOI at these sites (Table 3; eq.1). Conversely, fitted coefficient 'a' values for South River and East River BD models were positive (Table 3), demonstrating a positive relationship between H and BD at these sites. However, only the fitted coefficient 'a' for the East River model demonstrated a significant p-value. Westport and Hempstead fitted values for coefficient 'a' varied, but overall models at these sites did not perform as well. Additionally, almost all fitted model coefficients 'b' and 'c' from individual-site LOI models were positive values and revealed that model parameters Dc and De share a positive correlation with LOI across all sites (Table 3; eq.1). Conversely, 'b' and 'c' coefficients were mainly negative values in all BD models, suggesting that Dc and De

share an inverse relationship with BD. In all individual-site models coefficient 'b' demonstrates significant p-values ($P<.001$), suggesting that model parameter Dc, distance to tidal creeks, is a consistent predictor of spatial variability of sediment characteristics through these models.

Focusing specifically on South River models, model coefficients 'b' and 'c' have the smallest significant p-values and therefore suggest Dc and De model parameters demonstrate the strongest influence in predicting spatial variability of LOI and BD at that site. For East River models, coefficient values and corresponding p-values suggest H and Dc influence LOI most, and all model parameters significantly impact BD, with most influence given to Dc. Looking across other individual-site models at Westport and Hempstead, coefficient 'b' consistently demonstrates smallest significant p-values, suggesting Dc is the most important predictor of spatial variability of sediment characteristics in these models.

3.5 Cross-Site Model Results

The simple cross-site model based solely on equations 1 and 2 to predict soil properties revealed significant differences across marsh sites and resulted in low R^2 values for predicted LOI, BD, and CD ("Cross site" row of plots in Figure 6; Table 3). Predicted cross-site ranges of sediment characteristics were smaller than measured ranges, particularly for BD. Measured ranges of BD across sites were approximately 0.1-0.7 g/cm^3, whereas predicted BD only ranged from 0.15-0.25 g/cm^3. Variation in model success to predict LOI, BD, and CD across sites is evident in Figure 6 with each site's data points symbolized differently.

The addition of marsh distance to the inlet and local tidal range as parameters to the cross-site models improved results and accounted for some cross-site differences. A single value for marsh distance to the inlet and a single value for tidal range were calculated for each site (Table 1). South River, Westport, and Hempstead marsh sections demonstrated sites located further from the inlet (> 2800 m), while East River marsh is located closer to the inlet (128 m), and potentially closer to marine sediment sources. The highest median bulk density was also measured at East River marsh samples (Table 2). South River marsh exhibited a much larger tidal range (2.7 m) in comparison to other sites (0.93-1.6 m), and therefore experiences greater tidal inundation (Figure 1; Figure 4) and greater potential for sediment trapping. Distance to the inlet and tidal range values for each marsh site were added to Equations 1 and 2 as fourth and fifth model parameters, Di and TR. This resulted in a new cross-site model equation (eq.4) with an additional two fitted model coefficients, d and f.

All fitted model coefficients a, b, c, d, and f for new cross-site models exhibit significant p-values (P<.001; Table 3). Therefore, all morphometric model parameters, H, Dc, and De, as well as added regional parameters, Di and TR, are important predictors of LOI, BD, and CD. Coefficient ‘a’ values in the new cross-site models suggest an inverse relationship between H and LOI and a positive relationship with H and BD. Values for coefficients ‘b’ and ‘c’ demonstrate Dc and De both exhibit positive relationships with LOI and negative relationships with BD. Coefficients ‘d’ and ‘f’ confirm distance to the inlet and tidal range are important predictors of regional variability of sediment characteristics. All cross-site R^2 values improved and RMSE values decreased with the

addition of these two parameters and predicted ranges of sediment characteristics better reflected measured ranges.

3.6 Spatial Maps

Figure 7 shows that the calculated spatial patterns of sediment characteristics are the result of the combined influence of individual-site model parameters, H, Dc, and De. We were able to create predictive spatial maps based on these morphometric parameters for two sites where the model performed well, South River and East River (average $R^2 > 0.43$). Here, we use results from our LOI method and individual-site models as a proxy for grid-based mapping of soil organic matter (SOM) across each marsh (Figure 7, panels a and d). We also map grid-based spatial variability of BD and CD (Figure 7, panels b, e and c, f). According to ANOVA for the grid-based mapping, South River had a significantly higher mean modeled SOM throughout the marsh than East River (SR, 31% > ER, 19%; $P<.001$). Additionally, the mean predicted BD in East River marsh is significantly higher than South River (ER, 0.41 g/cm^3 > SR, 0.23 g/cm^3; $P<.001$). The variation in average predicted grid-based CD across these two sites is smaller, yet still statistically significant (ER, 0.034 gC/cm^3 > SR, 0.031 gC/cm^3; $P=0.01$). Overall, South River has a slightly larger range of predicted CD than East River, with the highest modeled CD values adjacent to South River uplands (Figure 7c). While mean values are presented in Figure 7, median values of predicted grid-based SOM, BD, and CD mapping are as follows: (SR: 28% SOM, 0.22 g/cm^3 BD, 0.03 gC/cm^3; ER: 19% SOM, 0.34 g/cm^3, 0.03 gC/cm^3). These grid-based median values are fairly representative of our measured median values for collected marsh samples (Table 2). Therefore, sampling distributions and resulting measured SOM, BD, and CD values for South River and East

River marsh sites provided a solid foundational dataset for morphometric models to be established and spatial maps to be created.

CHAPTER 4
DISCUSSION

4.1 Spatial Trends in Marsh Sediment Characteristics with Morphometric Parameters

Observed spatial patterns in soil properties across a given marsh reflect the interplay between belowground biomass production, mineral sediment accretion, and compaction. Increased proximity to the estuarine mouth, the marsh edge, and creeks all drive increases in sediment delivery (Christiansen et al., 2000; Moskalski & Sommerfield, 2012; Temmerman et al., 2003). Due to the higher packing density of mineral sediment relative to organic sediment (Morris et al., 2016; Neubauer 2008), these areas have higher resultant bulk densities. Further from sediment sources, i.e., increased Dc and De, in situ organic matter production by vegetation communities becomes more important for marsh vertical accretion. And while there is some disagreement regarding the relationship between bioproductivity and inundation, two microcosm studies from the region have shown that increased belowground biomass tends to increase with less inundation (Payne et al., 2019; Watson et al., 2017).

Factors controlling the observed spatial trends in sediment characteristics can be integrated and captured with our tested multivariate morphometric models. Within a single marsh site, SOM, BD, and CD can be modeled by tidal inundation above mean high water, distance from tidal creeks, and distance from the marsh edge. In nearly all models, parameter Dc, representing distance from tidal creeks, had the most significant influence in predicting sediment characteristics. While morphometric parameters H and De were also generally found to be significant predictors, coefficient ‘b’ values for the

Dc factor from all but one individual-site model equation demonstrated the smallest and most significant p-values (P<.00001 Table 3).

Spatial variation of morphometric factors H, Dc, and De across a single marsh site affects the relative composition of soil organic and inorganic material. Mineral matter and organic matter in soils have their own unique packing densities which are dependent on the material's texture, density, and porosity as well as their packing arrangement. Organic soils typically contain more pore space and have much lower bulk density compared to mineral soils (NRCS, 2008). Based on the ideal mixing model (Adams, 1973), bulk volume of marsh soils approximates the summed packing densities of the organic and mineral components (Morris et al., 2016, Neubauer 2008). Packing density also typically increases with soil depth since subsurface layers have reduced organic matter and root penetration compared to surface layers (NRCS, 2008). Therefore, subsurface marsh soils contain less pore space and are subject to compaction with the weight of the soil and potentially tidal inundation above them. Results from this study show that tidally-driven mineral sediment delivery via creeks and captured in our model by the terms Dc and De, as well as increased marsh inundation, H, typically influence marsh oxidation and auto-compaction and allow for higher BD and mineral-rich surface soils near creek banks (Payne et al., 2019; Reed et al., 1999; Watson et al., 2017). High bulk density proximal to creek banks along with increased tidal inundation can cause poor movement of air and water through the soil and subsequent restrictions to root growth and organic contributions. It was found that high BD and mineral-rich sediment levels off within about 20m of tidal creeks, and therefore, as elevation increases moving upland, tidal inundation and mineral sedimentation decreases, vegetation becomes denser, and

sediment becomes more organic and porous. In Figure 8, we demonstrate the complexity of these intertwined biological, chemical, and physical processes and the effect they have on the spatial patterns of the organic to inorganic ratio of marsh sediment.

The organic content and bulk density of the marsh soil ultimately affects the carbon density in that location. However, while there are clear spatial trends for SOM and BD with morphometric model parameters within a site, the two patterns counteract each other so that spatial variability of CD is less predictable. Additionally, the range of CD is small and based on measurements, CD is spatially homogenous to some extent with the 25th-75th percentile of observed CD at all sites being 0.037-0.047 gC/cm^3. On average, CD increases only slightly with increasing Dc and De, and decreasing H. With all marsh sites' CD values ranging from 0.03-0.05 gC/cm^3 (Figure 3; Table 2), the minute variation in CD supports the potential for using a mean CD value to map SOC at the marsh or regional scale.

4.2 Marsh Morphology and Regional Factors

Looking across marsh sites, marsh morphology, morphometric parameter ranges, sediment supply, tidal range and other site characteristics may play a role in model performance and regional variability of carbon stocks. The influence of marsh morphology is a combination of marsh estuarine and geologic setting, distance from the inlet, and structure of the tidal creek network. We found that single channel networks, like at South River and East River marsh, are more predictable and quantifiable by our morphometric model than systems like Westport and Hempstead with a higher density of sub-creek networks and ditches. The single channel network structure is reflected in the larger ranges of parameters Dc and De at South River and East River relative to those at

Westport and Hempstead. The small ranges in Dc and De at Westport and Hempstead are likely due to their morphology as well as smaller tidal range. Smaller parameter variation explains difficulties in model performance in predicting sediment characteristics. Morphometric metrics like De and Dc are also more comparable across sites with one main channel vs. sites with multiple sub-creek networks and extensive ditching. This finding supports the marsh management technique of restoring single channel hydrology (Adamowicz & Roman, 2005; Adamowicz et al., 2020; Wilson et al., 2014), especially when referencing restoration of frequent historical agricultural ditches in northeast salt marshes, as seen at Westport and Hempstead. The role of the tidal creek network and morphometric parameters H, Dc, and De in predicting SOC and other sediment characteristics is also somewhat dependent on adequate local sediment supply and delivery to the marsh.

Estuarine setting of a marsh, such as proximity to the inlet and exposed area of the marsh edge may also pose important predictors of marsh sediment characteristics and carbon stocks. For example, the East River marsh is located right at the inlet and demonstrated the highest bulk density and lowest SOM and CD, likely due to significant marine mineral sediment sourcing via a main tidal channel directly connected to the coast (Baranes et al., 2022). South River represents a wave-protected marsh site that also typically relies on marine sediment delivery and distribution via a large tidal range and a simple dendritic creek network morphology (Fitzgerald et al., 2020a; Reed et al., 1999). In contrast, Westport and Hempstead marshes are highly exposed systems located within large open embayments and largely lack well-developed creek systems. Both marshes have similar ratios of high SOM and low BD, potentially due to inadequate mineral

sediment delivery via a main tidal creek network (Rinaldo et al., 1999; Zeff, 1988). Instead, these types of multi-creek embayment marshes typically rely on storm surge and waves as dominant agents for marsh edge erosion and subsequent sediment delivery to the marsh platform (Cahoon, 2006; Reed, 1989; Turner et al., 2006). Uneven soil organic to inorganic ratio may therefore be a function of marsh location and morphology and potentially indicate signs of a degrading marsh (Morris and Bowden, 1986; Morris et al., 2016), unable to maintain pace with sea level rise and overall inorganic accretion, which in turn help preserve organic carbon stocks (Pace et al., 2021; Peteet et al., 2018).

Tidal range also impacts morphometric parameters and subsequently, predicted sediment characteristics. The local tidal range and mean marsh platform elevation affect the amount and duration of tidal inundation. The larger tidal range at South River relative to our other three sites resulted in greater tidal inundation above MHW, and potentially increased sedimentation. A larger tidal range is also thought to make marshes more resilient to sea level rise, assuming the existing marsh platform is generally stable (Fagherazzi et al., 2012; Kirwan et al., 2010). The larger tidal range and resulting larger range of H values at South River also explains greater model success in predicting spatial variability of SOC at this site. H incorporates a lot of information about a marsh, including the tidal range, MHW, and spatial variability of marsh platform elevation and tidal inundation. Overall, marshes with a larger tidal range and greater tidal inundation, assuming an adequate sediment supply, may be able to accumulate larger amounts of sediment quickly and systematically (Friedrichs & Perry, 2001; Reed, 1990), and therefore bury and store carbon more efficiently than those with a smaller tidal range.

4.3 Regional Models and SOC Mapping

Regional morphometric models with the addition of tidal range and distance to the inlet parameters greatly improved prediction of sediment characteristics at our marsh sites. The regional morphometric model based on H, Dc, and De parameters alone did not perform well. Poor performance of those cross-site models suggested challenges in comparing marshes of varying morphology and estuarine settings. Additional metrics comparable across marshes on a regional scale should be considered for future modeling efforts. These may include metrics to broadly categorize marsh morphology and health, such as the unvegetated to vegetated ratio (UVVR; Ganju et al., 2017), vegetation and elevation distributions and corresponding ecotone boundaries (Correll et al., 2019; Stevens et al., 2022), sediment supply, offshore sediment concentrations and turbidity (Raposa et al., 2016), marsh core to edge ratio (Stevens & Shull, 2021), presence of tidal restrictions within marsh systems, and others.

Spatial modeling of SOM, BD, and SOC at marsh sites with best-performing morphometric models demonstrates the usefulness of this technique for blue carbon accounting and management purposes. Our model results suggest a higher success rate of predicting sediment properties and estimating carbon stocks at marsh sites with a marsh morphology characteristic of a single channel tidal network. While spatial mapping of SOM and BD is possible with R-squared results up to 0.70, SOC mapping combines the challenges of opposing SOM and BD trends, therefore increasing mapping uncertainties. Spatial modeling can be successful at a marsh scale depending on morphology and health of marsh as well as success of proposed model metrics. Greater field sampling and measurements to support the building of empirical spatial models, such as our

morphometric model, increases mapping success as well. Specifically, regional SOC mapping may be more complicated and requires the addition of model metrics comparable across marsh sites. Model equations and methods from this study should be applied to other marshes to further validate successes or challenges in marsh-scale and regional carbon modeling.

4.4 Global Carbon Stock Comparison

Results from spatial maps created using morphometric models from this study produce comparable carbon stock values to other previous studies of marsh blue carbon. According to data from the IPCC (2013) published in the Blue Carbon Manual (Howard et al., 2014), average salt marsh carbon stocks are estimated as 255 Mg C/ha with a wide range of 16-623 Mg C/ha. These are globally averaged, area-based estimates of SOC stocks to 1 meter depth. SOM and BD vary predictably with depth, but since these two values are multiplied to obtain carbon density, CD remains fairly consistent with depth to 1m (Holmquist et al., 2018). Therefore, when applying a similar method to estimate total carbon stocks in our northeast U.S. marshes, we use the median grid-based predicted CD at each marsh site, which is a result of the individual-site model-based mapping. We obtained a carbon stock estimate of 304 Mg C/ha at the South River site and 298 Mg C/ha at our East River site when projecting surface values to 1m depths. These estimates are therefore higher than the global average carbon stock, and when converted to carbon density, indicate approximately 0.030 kg C/cm^3, or about 10% higher than the reported mean CD value of 0.027 kg C/m^3 for the continental US in Holmquist et al. (2018). Further, we know our model consistently underpredicted CD due to the counteracting spatial trends of SOM and BD. Therefore, measured mean CD from our northeast marsh

data results in an even higher value of 0.042 gC/cm^3 compared to various other published studies which range from 0.025-0.028 gC/cm^3 (Holmquist et al., 2018; IPCC, 2013; Nahlik & Fennessey, 2016; van de Broek et al., 2016). If we were to use measured mean CD from this study to estimate carbon stocks to 1m, we would obtain an average carbon stock of 420 Mg C/ha in northeast marshes, which is on the higher end of global estimates.

While these results show that our morphometric model is an acceptable and comparable method for carbon accounting at the marsh-scale, for the purpose of calculating whole marsh carbon stock and sequestration values, using a regionally appropriate value may be preferable. However, while estimating SOC to 1m depth is a common practice in marsh blue carbon accounting, previous studies have shown that northeast marshes can be up to several meters deep, potentially resulting in a significant underestimate of total carbon stocks (Pace et al., 2021; Peteet et al., 2020; van Ardenne et al., 2018). Conversely, there is potential marsh peat can be less than 1m depth, not only system-wide, but with more shallow deposits of sediment towards landward limits. While this study was focused on quantifying relationships between present day morphometric parameters and surface soil properties, we encourage future full-marsh carbon stock accounting efforts to consider variability of peat depth.

The IPCC (2013) also reports that based on a conversion factor, the average salt marsh carbon stock of 255 Mg/ha, has a CO_2 equivalent of 935 Mg CO_2/ha of potential emissions. At our South River site, we estimate 1116 Mg CO_2/ha emission potential and 1094 Mg CO_2/ha at East River. These are the estimated CO_2 re-emissions if all the organic carbon in the upper 1m of sediment becomes oxidized. Marsh peat oxidation is

especially a concern with increasing anthropogenic coastal development, tidal restrictions, and other alterations of tidal hydrology, as well as natural marsh compaction and subsidence over time. Overall, our comparison to IPCC blue carbon estimates indicates that salt marshes in the northeast U.S. are efficient carbon-sequestering and carbon-burying ecosystems.

4.5 Trade-offs of Process-Based Approach

A major question that arises from previous blue carbon accounting studies is whether a process-based approach is more accurate and efficient for spatial mapping of carbon stocks rather than the assumption of a simple mean carbon density value. Specifically, Holmquist et al. (2018) identified using a mean carbon density value as the simplest and best-performing strategy for predicting and mapping carbon stocks in the conterminous U.S. We examined the difference between our morphometric spatial modeling method and the Holmquist method by calculating the mean absolute percentage error (MAPE) of observed versus predicted carbon density values for both methods on our data. Across all four marsh sites, our method results in lower MAPEs than the Holmquist method of using the mean CONUS CD of 0.027 gC/cm^3. For example, our method resulted in CD MAPEs of 14-26% (Table 2) whereas applying the Holmquist method resulted in MAPEs of 29-40%. Therefore, our method outperformed the Holmquist method tested on our field sampling dataset. This suggests there are benefits to applying a more detailed spatial approach than just applying Holmquist's single value for predicted carbon density when mapping carbon stocks in northeast marshes. However, since Holmquist used the mean carbon density from samples collected across the entire conterminous U.S., we calculated the mean CD measured across our four sites to account for regional variation in the single

value method. Mean CD from soil samples at our four sites was significantly higher (0.042 gC/cm^3) and using this single value instead of Holmquist's value resulted in MAPEs of 12-17% at each of our sites. In this case, the single northeast mean CD value method outperformed the morphometric method at 3 out of 4 sites. Future carbon stock mapping efforts at the regional scale may want to consider convenience, economical, and precision tradeoffs in implementing either the single regional CD value method or a more process-based approach.

4.6 Management Implications

Accelerating global sea level rise may allow for greater inundation of marshes, promoting increased and quickened sediment accumulation (D'Alpaos et al., 2011; Kirwan et al., 2016; Morris et al., 2002; Mudd et al., 2009), resulting in additional capacity for carbon storage. Increased atmospheric concentrations of CO_2, also contributing to sea level rise, have shown increased biological plant response of organic elevation gain as well in marshes (Langley et al., 2009). However, more recent studies have shown that marshes might not be resilient to increasing rates of sea level rise compounded with wave-induced coastal erosion (IPCC, 2013), marsh subsidence, and additional stressors (Crosby et al., 2016; Day & Templet, 2008; Kearney et al., 2011; Vinent et al., 2021). Improved methods for sediment and carbon storage accounting as proposed in this study are necessary as a means to stimulate projects and secure funding for coastal intervention. This study also highlights the promising management technique of restoring single-channel hydrology to marshes, resulting in more natural and predictable sediment and carbon dynamics. Implementing proper hydrology must be coupled with maintaining adequate sediment supply along coastlines to provide marshes a chance to maintain and

build elevation and preserve related carbon stocks (Fitzgerald & Hughes, 2019; Weston et al., 2014). Therefore, coastal armoring, shoreline development, and tidal river barrier projects at municipal to federal scales must be seriously considered in order to weigh costs and benefits of resilience for both humans and natural coastal resources like salt marshes. If nothing is done, sea level rise and associated impacts of climate change are a dangerous threat to the destruction and drowning of marshes as well as the potential re-emission of greenhouse gasses from marsh soil carbon repositories built up over thousands of years. A call to action is needed now in order to preserve marshes and their invaluable abilities to protect coastlines against storm surge flooding, sequester and store vast amounts of carbon, filter runoff and pollutants, provide nursery grounds for various wildlife, and foster aesthetic and recreational benefits. Overall, results from this study pose a greater science justification for proper management of northeast coastal lands and infrastructure and the vulnerable natural ecosystems, like salt marshes, that depend on them.

CHAPTER 5
CONCLUSION

There are tradeoffs in methods of carbon stock prediction and mapping. The selection of a blue carbon modeling technique largely depends on the scale and proposed questions to be answered. A national mean value of carbon density has been considered sufficient for national-scale mapping of carbon stocks (Holmquist et al., 2018). However, we show here that carbon stocks vary within and between marshes within a region, providing motivation to rigorously map carbon at fine spatial resolution to aid in carbon accounting. Process-based approaches like our tested morphometric models may yield stronger spatial mapping accuracy of marsh-scale SOC, especially when applied in marsh sites of a single channel morphology. Future studies should further investigate the effects of distance from tidal creeks on SOC, as the variable Dc had the strongest influence in our proposed morphometric models. Other process-based spatial metrics in marshes to predict SOC at the marsh-scale may be worth investigating as well, particularly those that counteract the opposing spatial trends in soil organic matter and sediment bulk density. Regional-scale mapping of marsh SOC, on the other hand, may be sufficient and potentially more effective with the application of a regional mean CD value. To consider improving future estimations of full-marsh and regional carbon stocks, variability in the depth of peat sequence within and between marsh complexes is also of great interest. Overall, the tested morphometric parameters in our models confirmed and represented spatial variability of complex geomorphic and ecological processes involved in marsh carbon dynamics. Estimates of carbon stocks from this study are comparable to estimates provided in previous salt marsh studies. However, measured mean carbon density from our northeast marsh data is much higher compared to various other published studies.

Therefore, larger carbon storage capacity in northeast marshes should provide greater justification for fine-scale carbon mapping and protecting and managing these ecosystems and associated carbon stocks.

CHAPTER 6
TABLES AND FIGURES

Table 1. Site Summary: Marsh location, morphology, tidal characteristics, and lidar-DEM origin.

Site	Location	Morphology	Mean Tidal Range (m)	MHW (m)	Distance to Inlet (km)	RTK Median H (m)	Lidar Median H (m)	Lidar Data Origin
South River	Marshfield, MA	Back-barrier fluvial	2.7	1.3	4.5	0.095 ± 0.11	0.088 ± 0.18	2013-14 USGS Post Sandy Lidar (0.35 m)
East River	Guilford, CT	Fluvial tidal river	1.6	0.79	0.13	-0.068 ± 0.098	-0.083 ± 0.082	2016 Connecticut Statewide Lidar
Westport	Westport, MA	Partially-exposed fringing	0.93	0.31	2.8	-0.082 ± 0.023	-0.088 ± 0.082	2013-14 USGS Post Sandy Lidar
Hempstead	Long Island, NY	Islands in back-barrier lagoon	1.4	0.55	3.6	-0.088 ± 0.059	-0.13 ± 0.26	2011-12 NYSDEC Lidar: Coastal New York

Note. H is tidal inundation above local mean high water (MHW-elevation). Median H values reported with standard deviations. Lidar data sources include: 2013-2014 U.S. Geological Survey CMGP LiDAR: Post Sandy (MA, NH, RI) from 2010-06-15 to 2010-08-15. NOAA National Centers for Environmental Information, https://www.fisheries.noaa.gov/inport/item/49846; Connecticut Statewide Lidar DEM 2016 from 2010-06-15 to 2010-08-15. NOAA National Centers for Environmental Information, https://www.fisheries.noaa.gov/inport/item/49408; and 2011 - 2012 New York State Department of Environmental Conservation (NYSDEC) Lidar: Coastal New York (Long Island and along the Hudson River) from 2010-06-15 to 2010-08-15. NOAA National Centers for Environmental Information, https://www.fisheries.noaa.gov/inport/item/49888.

Table 2. Intersite Comparison of Sediment Characteristics and Model Errors: Including observed (obs) and model predicted (pred) sediment characteristics with mean absolute percentage errors (MAPEs) for LOI, BD, and CD models.

Site	LOI			BD			CD		
	Median Obs (fraction)	Median Pred (fraction)	MAPE (%)	Median Obs (g/cm^3)	Median Pred (g/cm^3)	MAPE (%)	Median Obs (gC/cm^3)	Median Pred (gC/cm^3)	MAPE (%)
South River	0.34	0.25	26.6	0.23	0.23	21.1	0.040	0.029	25.5
East River	0.19	0.18	17.8	0.44	0.40	13.9	0.039	0.035	14.0
Westport	0.50	0.40	23.6	0.17	0.17	18.3	0.041	0.033	20.3
Hempstead	0.50	0.46	15.2	0.18	0.17	16.7	0.047	0.039	17.0

Note. The equation for MAPE is: $(1/n) * \Sigma (|observed - predicted| / |observed|) * 100$.

Table 3. Morphometric Model Results: Model coefficients, corresponding p-values, R-squared values, and Root Mean Square Error (RMSE).

Model	LOI								BD								CD	
	k *(p-value)*	a *(p-value)*	b *(p-value)*	c *(p-value)*	d *(p-value)*	f *(p-value)*	R^2	RMSE	k *(p-value)*	a *(p-value)*	b *(p-value)*	c *(p-value)*	d *(p-value)*	f *(p-value)*	R^2	RMSE	R^2	RMSE
South River	0.0270 *(0.799)*	**-1.0501** *(4.5e-11)*	**0.0097** *(0.000)*	**0.0007** *(0.000)*	---	---	0.68	0.107	**1.2452** *(0.000)*	0.0643 *(0.671)*	**-0.0053** *(1.1e-13)*	**-0.0005** *(0.000)*	---	---	0.43	0.119	0.25	0.012
East River	**0.1335** *(0.015)*	**-0.7356** *(3.8e-5)*	**-0.0060** *(0.000)*	3.0e-7 *(0.989)*	---	---	0.48	0.057	**0.7595** *(1.4e-11)*	**0.7458** *(4.3e-4)*	**-0.0065** *(8.0e-15)*	**-0.0001** *(6.9e-6)*	---	---	0.70	0.072	0.11	0.009
Westport	**0.3661** *(1.5e-8)*	**-0.3272** *(0.036)*	**0.0060** *(2.0e-8)*	**0.0003** *(2.1e-4)*	---	---	0.11	0.124	**0.1994** *(5.3e-10)*	**-0.2080** *(0.007)*	**-0.0044** *(7.0e-15)*	**-0.0002** *(2.7e-6)*	---	---	0.09	0.061	0.01	0.012
Hempstead	**0.3663** *(9.5e-9)*	0.4837 *(0.081)*	**0.0172** *(4.9e-6)*	0.0001 *(0.541)*	---	---	0.16	0.093	**0.1866** *(5.7e-8)*	-0.0032 *(0.983)*	**-0.0102** *(1.2e-6)*	**0.0001** *(0.007)*	---	---	0.08	0.051	0.04	0.009
Cross-site	**0.3846** *(0.000)*	0.0070 *(0.955)*	**0.0023** *(2.3e-5)*	**-0.0003** *(0.000)*	---	---	0.12	0.186	**0.1829** *(0.000)*	**0.7273** *(2.8e-15)*	-0.0007 *(0.062)*	**3.0e-5** *(0.003)*	---	---	0.14	0.134	0.01	0.019
Cross-site + Di + TR	**0.3011** *(2.4e-14)*	**-0.9856** *(0.000)*	**0.0072** *(0.000)*	**0.0002** *(0.000)*	**0.0003** *(0.000)*	**-0.8121** *(0.000)*	0.52	0.131	**0.2326** *(0.000)*	**0.5263** *(1.7e-14)*	**-0.0052** *(0.000)*	**-0.0002** *(0.000)*	**-0.0003** *(0.000)*	**0.7465** *(0.000)*	0.55	0.092	0.08	0.013

Note. Coefficients a, b, c, d, and f correspond to model parameters H, Dc, De, Di, and TR, respectively, and 'k' represents the model intercept values (eq.1-4). Corresponding p-values are listed directly below all fitted model coefficient and intercept values. Bolded coefficient or intercept signifies a significant p-value ($P<0.05$). RMSE = $\sqrt{[\Sigma (P - O)^2 / n]}$ where P represents predicted values, O represents observed values, and n is the sample size. RMSE units for LOI, BD, and CD are fraction organic, g/cm^3, and gC/cm^3, respectively.

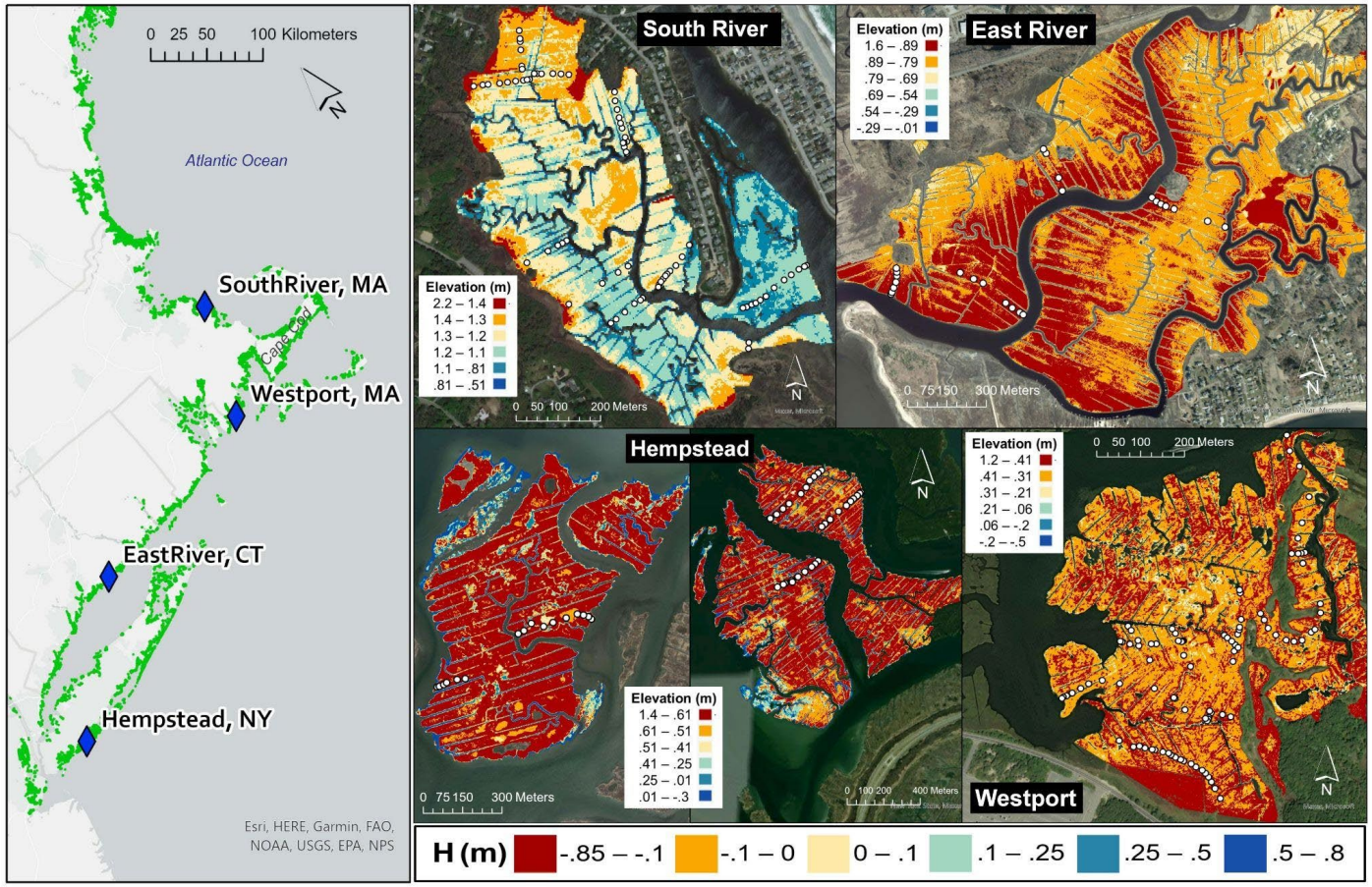

Figure 1. Study Sites: Tidal marsh study sites within the northeastern U.S. symbolized by H, which is tidal inundation based on lidar elevations (z) and each site's local mean high water (H = MHW-z). Marsh platform elevation relative to NAVD88 also included with different scale bars for each site. Elevation derived from various sources of lidar downloaded from NOAA Digital Coast Data Access Viewer (https://coast.noaa.gov/dataviewer). MHW values derived from Yellen et al., (2023) for the South River site, and National Geodetic Survey records (https://geodesy.noaa.gov/NGSDataExplorer/) and NOAA tidal datums (https://tidesandcurrents.noaa.gov/stations.html?type=Datums) for the other marsh sites. Sediment sampling locations depicted by black and white points.

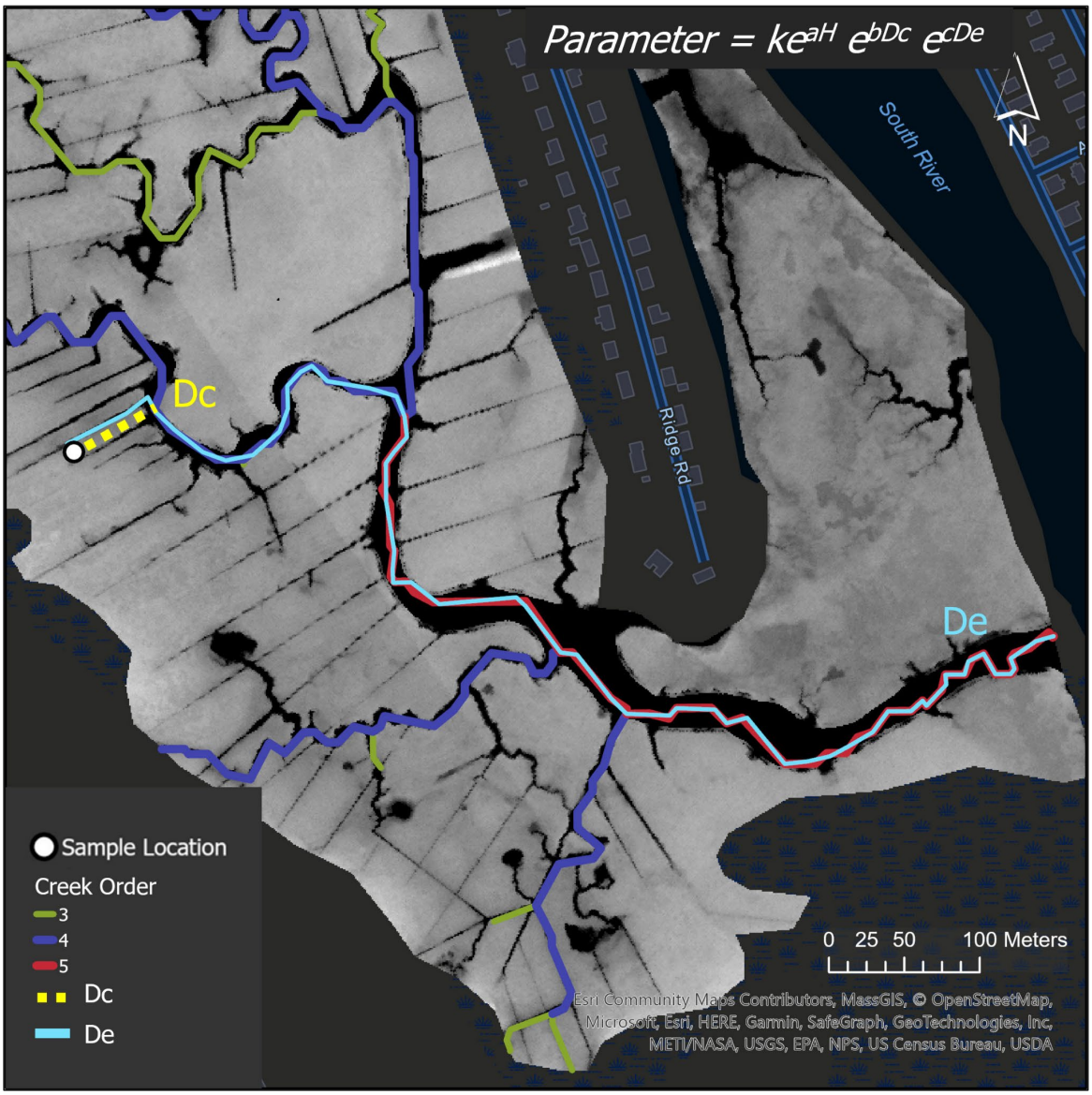

Figure 2. Example of Model Parameter Extraction: Visual depicting derived morphometric model parameters for a sample at South River marsh. Lidar clipped to marsh extent using USFWS National Wetlands Inventory 'Estuarine and Marine Wetland' classes (https://www.fws.gov/program/national-wetlands-inventory), with main tidal creeks delineated using ArcGIS Pro Hydrology tools. Distance from the sample location to the nearest tidal creek, Dc (yellow dashed) and distance to the marsh edge, De (light blue solid) indicated on map.

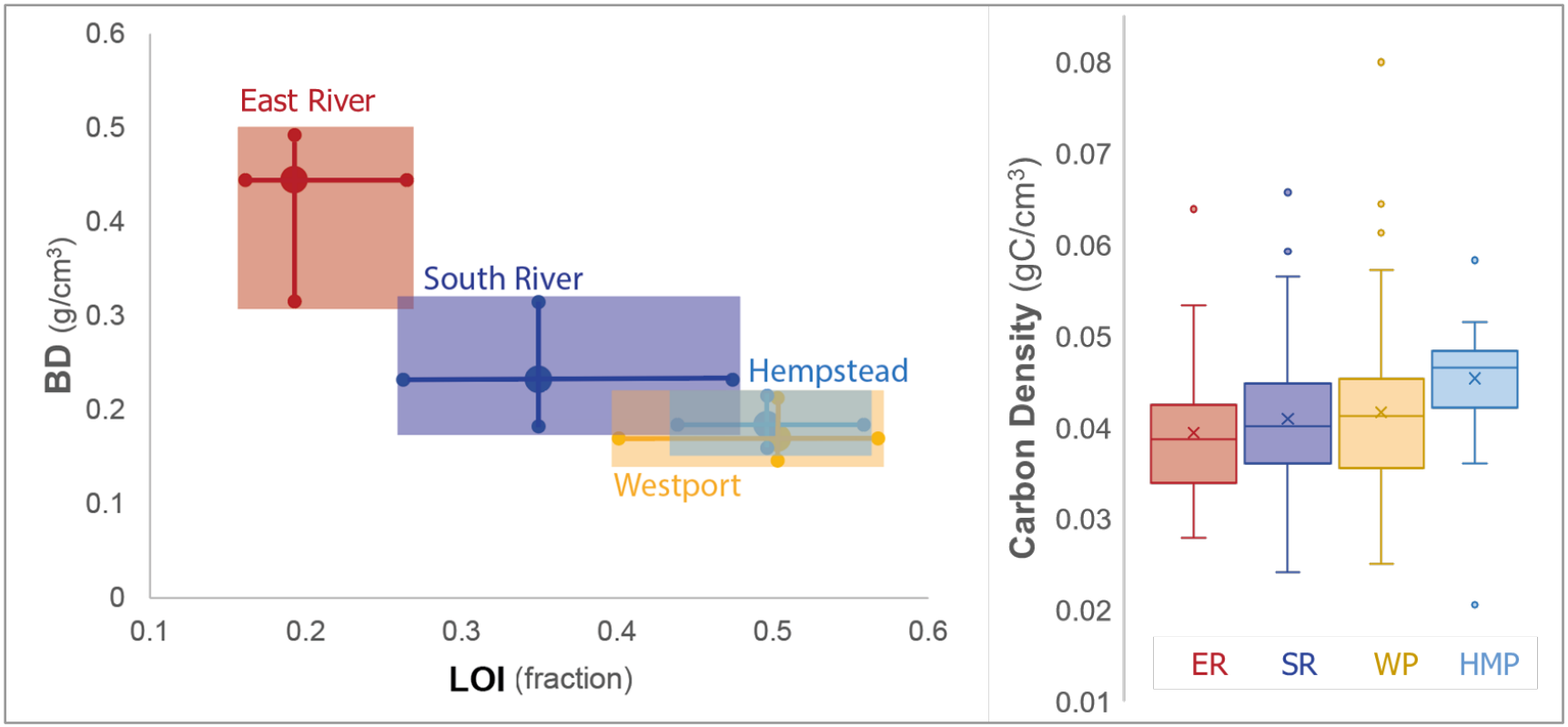

Figure 3. Intersite Comparison of Sediment Characteristics: Variation in measured sediment characteristics within and across marsh sites. Center data points within boxes represent median LOI and median BD at each site. Boxes represent the 25th to 75th percentile range of LOI and BD at each site. Median observed carbon density (CD) is presented for each site.

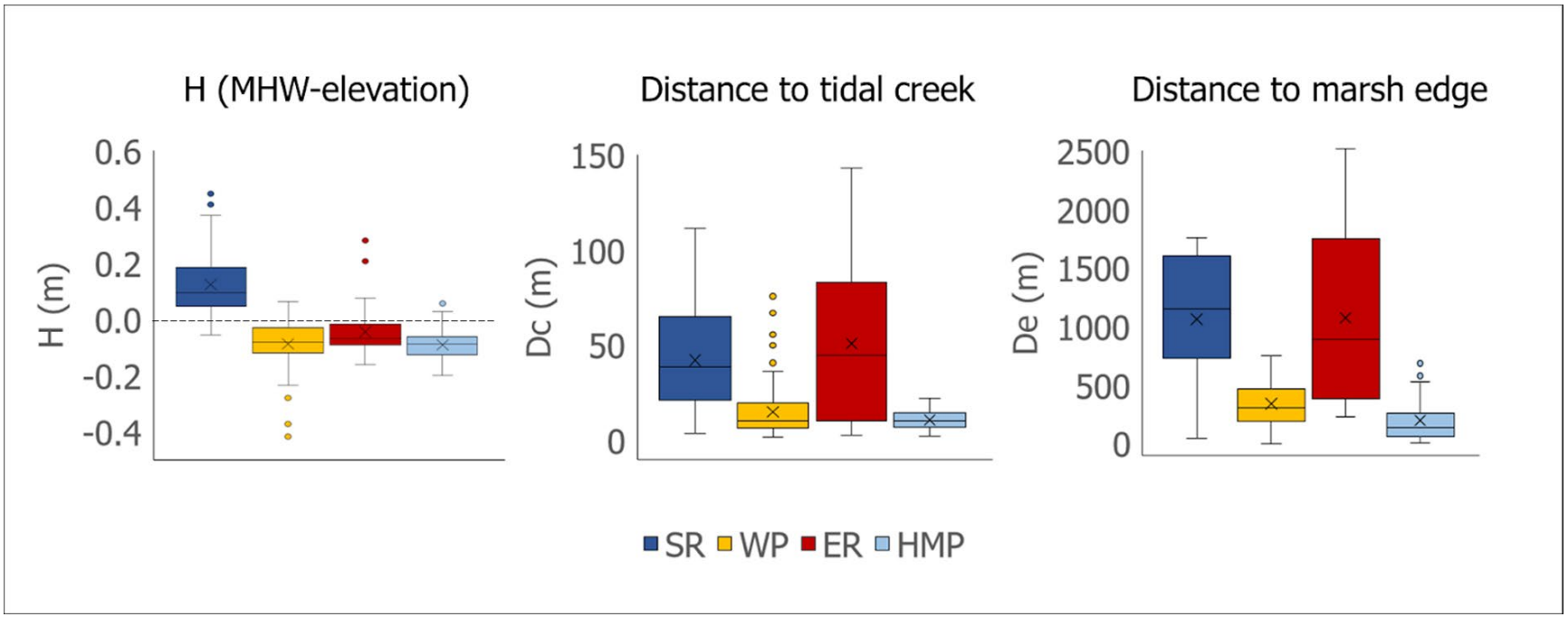

Figure 4. Variation in Morphometric Parameters at Marsh Sampling Locations: Boxplots represent distribution of derived morphometric model parameters at sample locations within our four northeast marsh site sections, including H (MHW-elevation), Dc (distance to the nearest tidal creek), and De (distance to the marsh edge). Values calculated using RTK-surveyed sampling locations and ArcGIS Pro hydrology tools. Dotted line at H=0 on the far left plot indicates threshold for tidal inundation above or below MHW.

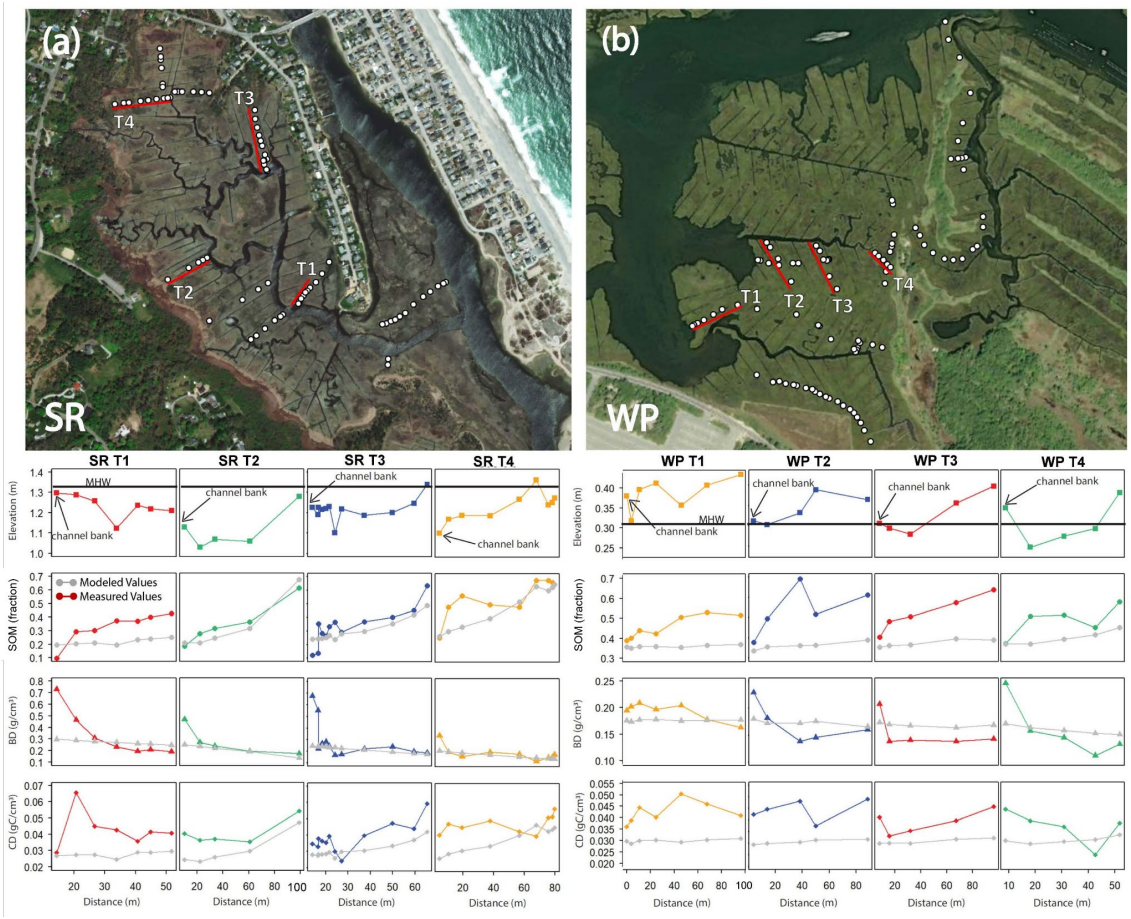

Figure 5. Spatial Relationships with Distance from Creeks along Selected Transects: South River and Westport marshes with elevation and marsh sediment characteristics plotted as a function of distance from the tidal creek, Dc. Each site also demonstrates increasing distance from the marsh edge, De, values when progressing from Transect 1 to 4. Measured values of elevation, soil organic matter (SOM), bulk density (BD), and carbon density (CD) at each sampling location along the transects are shown in color. Corresponding modeled values for the same locations based on individual-site morphometric models are shown in gray. Mean high water (MHW) for each site represented by black solid line to demonstrate H (tidal inundation above MHW)

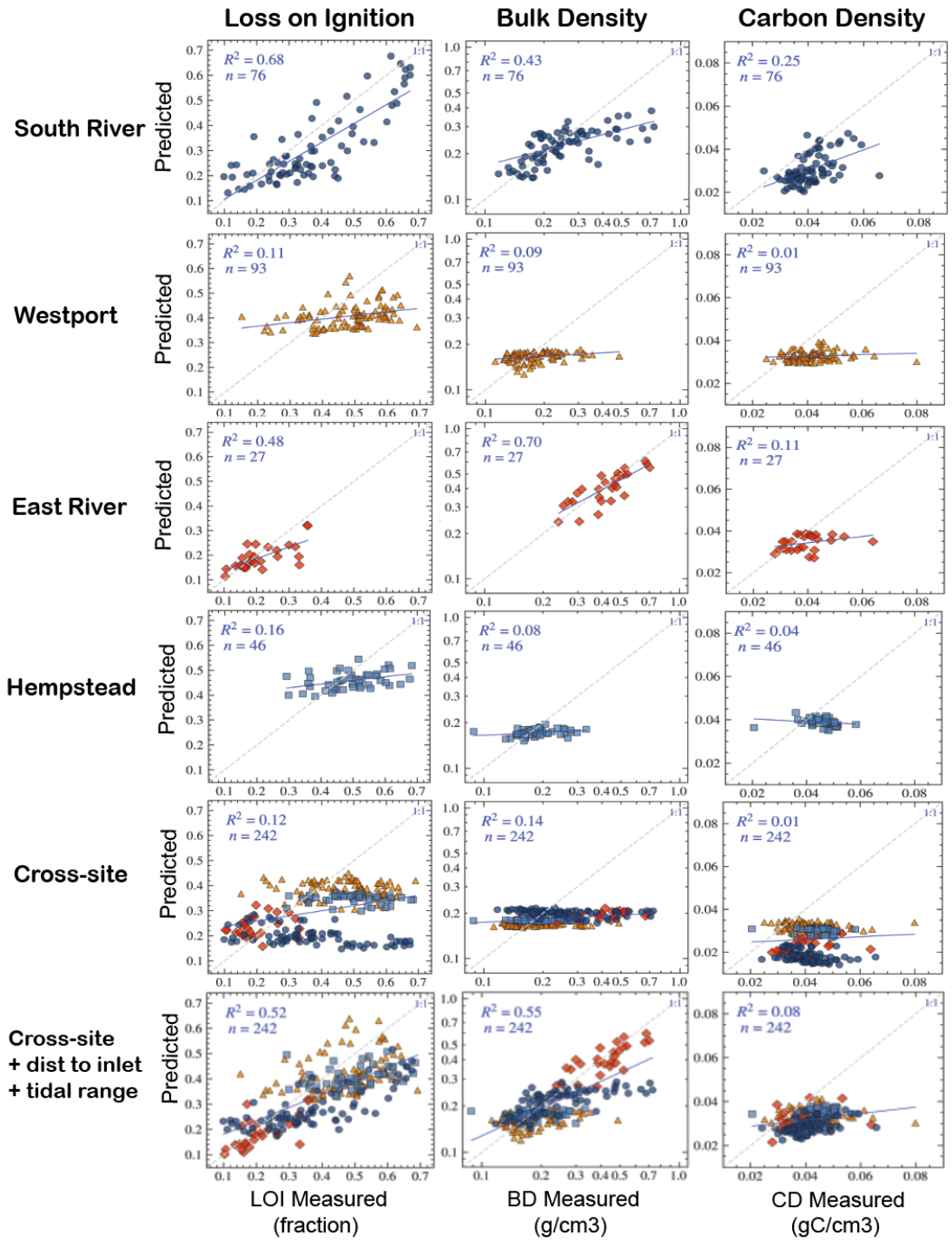

Figure 6. Morphometric Model Results for Individual-Site and Cross-Site Models: Regression results in rows 1-5 are from the regression model described by eq.1-eq.3. Regression results in row 6 are from the regression model described by eq.4, with distance to the inlet and tidal range model parameters added to account for cross-site differences. Plots include measured values versus predicted model values for LOI, BD, and CD, with R-squared values for each plot reported.

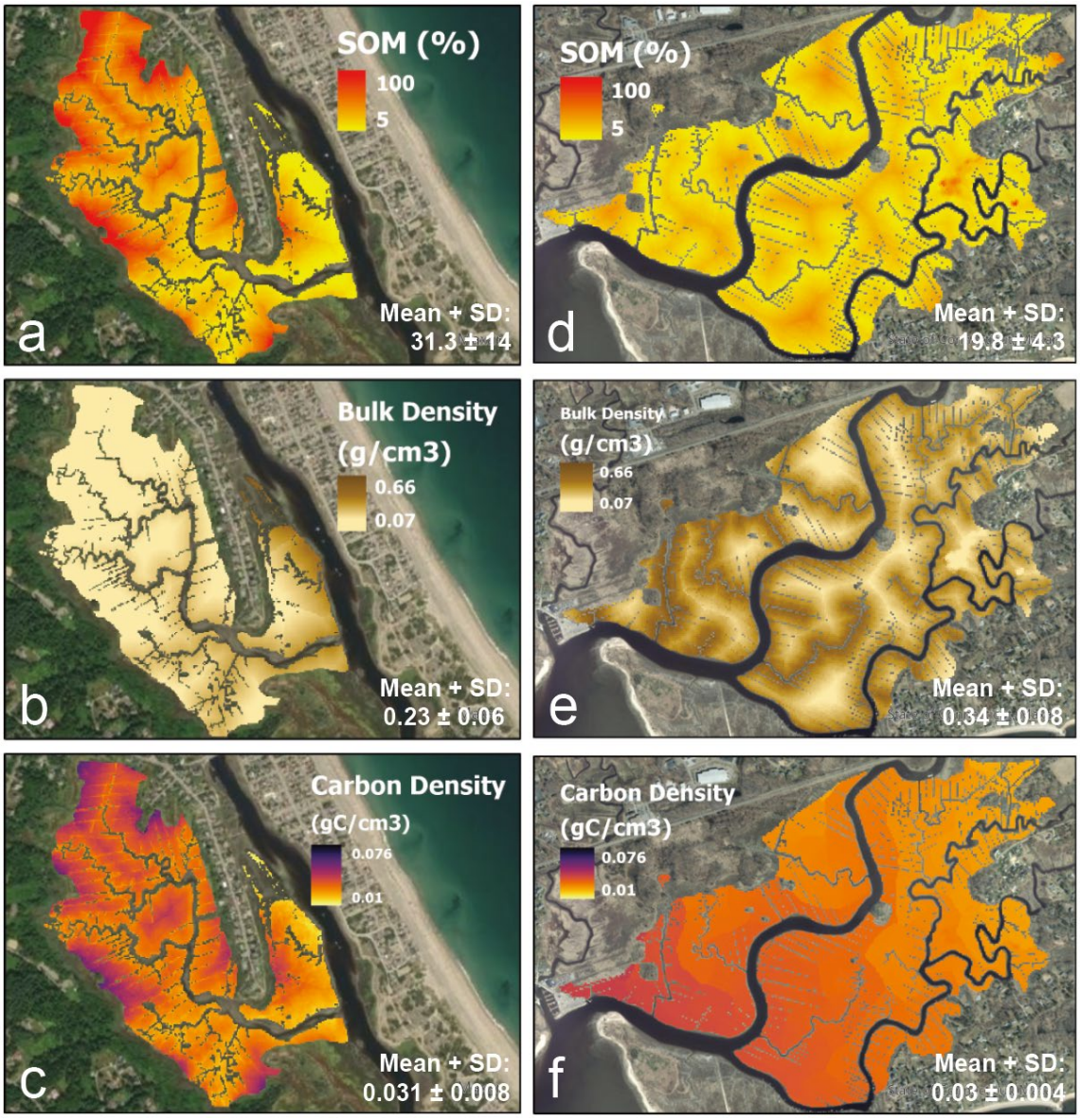

Figure 7. Spatial Maps of Soil Organic Matter, Bulk Density, and Carbon Density: Model-predicted spatial variability of SOM, BD, and CD across the South River marsh (panels a-c) and East River marsh (panels d-f) sites. Values were calculated for each marsh platform grid cell based on the individual-site morphometric models. For comparison, the scale of color bars for SOM, BD and CD are the same for left and right plots. Predicted mean and standard deviations are reported.

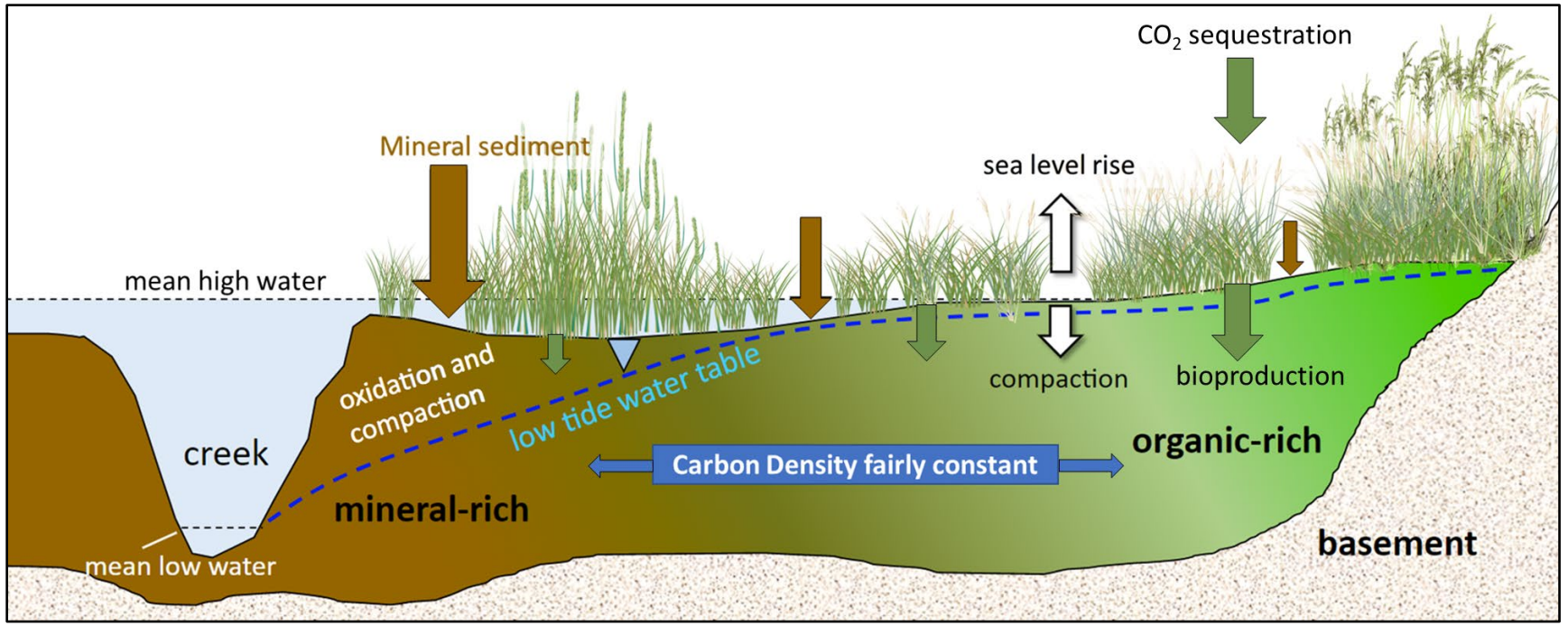

Figure 8. Tidal Marsh Carbon and Sediment Dynamics Diagram: Tidal marsh platform with sediment characteristics as a function of distance from tidal creeks, tidal inundation, and elevation and vegetation structure. Some of these dynamics are represented by morphometric model parameters from this study. Other relevant physical, chemical, and biological processes are depicted.

APPENDIX

SUPPLEMENTARY FIGURES

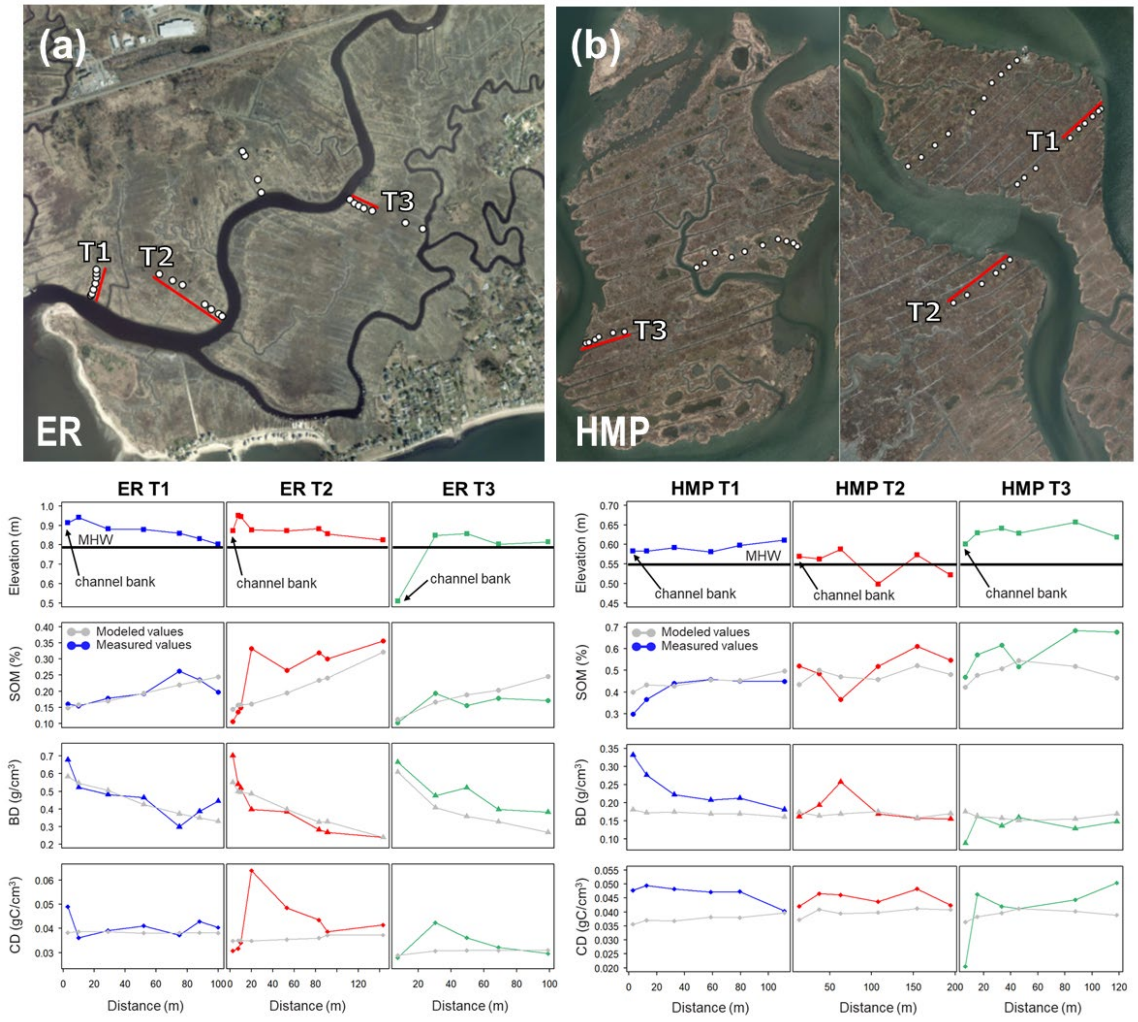

Figure S1. Selected transects from East River and Hempstead marshes with elevation and marsh sediment characteristics plotted as a function of distance from the tidal creek, Dc. Each site also demonstrates increasing distance from the marsh edge, De, values when progressing from Transect 1 to 3. Measured values of elevation, soil organic matter (SOM), bulk density (BD), and carbon density (CD) at each sampling location along the transects are shown in color. Corresponding modeled values for the same locations based on individual-site morphometric models are shown in gray. Mean high water (MHW) for each site represented by black solid line to demonstrate H (tidal inundation above MHW).

REFERENCES

Adamowicz, S.C., G. Wilson, D.M. Burdick, W. Ferguson, and R. Hopping. 2020. Farmers in the marsh: Lessons from history and case studies for the future. Wetland Science & Practice 183–195.

Adamowicz, S.C., Roman, C.T. 2005. New England salt marsh pools: A quantitative analysis of geomorphic and geographic features. Wetlands 25, 279–288. https://doi.org/10.1672/4

Adams, W. A. 1973. The effect of organic matter on the bulk and true densities of some uncultivated podzolic soils, Journal of Soil Science, 24, 10–17.

Allen, J. R. L. 2000. Morphodynamics of Holocene salt marshes: a review sketch from the Atlantic and Southern North Sea coasts of Europe. Quaternary Science Reviews, 19(12), 1155–1231. https://doi.org/10.1016/S0277-3791(99)00034-7.

Baranes, H. E., Woodruff, J. D., Geyer, W. R., Yellen, B. C., Richardson, J. B., and Griswold, F. 2022. Sources, mechanisms, and timescales of sediment delivery to a New England salt marsh. Journal of Geophysical Research: Earth Surface, 127, e2021JF006478. https://doi.org/10.1029/2021JF006478.

Barbier, E. B., Hacker, S. D., Kennedy, C., Koch, E. W., Stier, A. C., and Silliman, B. R. 2011. The value of estuarine and coastal ecosystem services. Ecological Monographs, 81(2), 169–193. https://doi.org/10.1890/10-1510.1.

Bear, J. 1972. Dynamics of Fluids in Porous Media. American Elsevier Publishing Company, New York, 764 p.

Bouillon, S., Dahdouh-Guebas, F., Rao, A. et al. 2003. Sources of organic carbon in mangrove sediments: variability and possible ecological implications. Hydrobiologia 495, 33–39. https://doi.org/10.1023/A:1025411506526.

Cahoon, D. R. 2006. A review of major storm impacts on coastal wetland elevations. Estuaries and Coasts, 29(6), 889– 898. https://doi.org/10.1007/BF02798648

Chmura, G. L., Anisfeld, S. C., Cahoon, D. R., and Lynch, J. C. 2003. Global carbon sequestration in tidal, saline wetland soils. Global biogeochemical cycles, 17(4).

Christiansen, T., Wiberg, P. L., and Milligan, T. G. 2000. Flow and Sediment Transport on a Tidal Salt Marsh Surface. Estuarine, Coastal and Shelf Science, 50(3), 315–331. https://doi.org/10.1006/ECSS.2000.0548

Connecticut Statewide Lidar DEM 2016 from 2010-06-15 to 2010-08-15. NOAA National Centers for Environmental Information,https://www.fisheries.noaa.gov/inport/item/49408.

Correll, M.D., Hantson, W., Hodgman, T.P. et al. 2019. Fine-Scale Mapping of Coastal Plant Communities in the Northeastern USA. Wetlands 39, 17–28. https://doi.org/10.1007/s13157-018-1028-3

Crosby, S. C., Sax, D. F., Palmer, M. E., Booth, H. S., Deegan, L. A., Bertness, M. D., and Leslie, H. M. 2016. Salt marsh persistence is threatened by predicted sea-level rise. https://doi.org/10.1016/j.ecss.2016.08.018.

D'Alpaos, A., Mudd, S. M., and Carniello, L. 2011. Dynamic response of marshes to perturbations in suspended sediment concentrations and rates of relative sea level rise. Journal of Geophysical Research: Earth Surface, 116(F4), 4020. https://doi.org/10.1029/2011JF002093.

Day, J. W., and Templet, P. H. 2008. Consequences of sea level rise: Implications from the mississippi delta. Http://Dx.Doi.Org/10.1080/08920758909362088, 17(3), 241–257. https://doi.org/10.1080/08920758909362088.

Dean, W. E. Jr. 1974. Determination of carbonate and organic matter in calcareous sediments and sedimentary rocks by loss on ignition: Comparison with other methods. J. Sed. Petrol. 44: 242–248.

Deegan, L. A., Johnson, D. S., Warren, R. S., Peterson, B. J., Fleeger, J. W., Fagherazzi, S., and Wollheim, W. M. 2012. Coastal eutrophication as a driver of salt marsh loss. Nature 2012 490:7420, 490(7420), 388–392. https://doi.org/10.1038/nature11533

Duarte, C., Losada, I., Hendriks, I. et al. 2013. The role of coastal plant communities for climate change mitigation and adaptation. Nature Clim Change 3, 961–968. https://doi.org/10.1038/nclimate1970

Duarte, C. M., Middelburg, J. J., and Caraco, N. 2005. Major role of marine vegetation on the oceanic carbon cycle, Biogeosciences, 2, 1–8. https://doi.org/10.5194/bg-2-1-2005

Ewers Lewis, C. J., Young, M. A., Ierodiaconou, D., Baldock, J. A., Hawke, B., Sanderman, J., Carnell, P. E., and Macreadie, P. I. 2020. Drivers and modelling of blue carbon stock variability in sediments of southeastern Australia. Biogeosciences, 17(7), 2041–2059. https://doi.org/10.5194/BG-17-2041-2020.

Fagherazzi, S., Kirwan, M. L., Mudd, S. M., Guntenspergen, G. R., Temmerman, S., D'Alpaos, A., Van De Koppel, J., Rybczyk, J. M., Reyes, E., Craft, C., and Clough, J. 2012. Numerical models of salt marsh evolution: Ecological, geomorphic, and climatic factors. Reviews of Geophysics, 50(1), 1002. https://doi.org/10.1029/2011RG000359.

FitzGerald, D., Ryerson, O., Hughes, Z., Black, S., Georgiou, I., Hein, C., and Novak, A. 2020. Long-term variability in inorganic sediment contributions to the Great Marsh, Massachusetts. Journal of Coastal Research, 95(SI), 490– 494. https://doi.org/10.2112/SI95-095.1

Fitzgerald, D. M., and Hughes, Z. 2019. Marsh Processes and Their Response to Climate Change and Sea-Level Rise. Https://Doi.Org/10.1146/Annurev-Earth-082517-010255, 47, 481–517. https://doi.org/10.1146/ANNUREV-EARTH-082517-010255.

FitzGerald, D. M., Hughes, Z. J., Georgiou, I. Y., Black, S., and Novak, A. 2020. Enhanced, climate-driven sedimentation on salt marshes. Geophysical Research Letters, 47, e2019GL086737. https://doi.org/10.1029/2019GL086737

Friedrichs, Carl T., and James E. Perry. 2001. "Tidal Salt Marsh Morphodynamics: A Synthesis." Journal of Coastal Research, pp. 7–37. JSTOR, http://www.jstor.org/stable/25736162.

Ganju, N., Defne, Z., Kirwan, M. et al. 2017. Spatially integrative metrics reveal hidden vulnerability of microtidal salt marshes. Nat Commun 8, 14156. https://doi.org/10.1038/ncomms14156

Gedan KB, Altieri AH, Bertness MD. 2011. Uncertain future of New England salt marshes. Mar Ecol Prog Ser 434:229-237. https://doi.org/10.3354/meps09084.

Geyer, W.R., Woodruff, J.D. and Traykovski, 2001. P. Sediment transport and trapping in the Hudson River estuary. Estuaries 24, 670–679. https://doi.org/10.2307/1352875

Gulliver, A., Carnell, P. E., Trevathan-Tackett, S. M., Duarte de Paula Costa, M., Masqué, P., and Macreadie, P. I. 2020. Estimating the Potential Blue Carbon Gains From Tidal Marsh Rehabilitation: A Case Study From South Eastern Australia. Frontiers in Marine Science, 0, 403. https://doi.org/10.3389/FMARS.2020.00403.

Holmquist, James R., Lisamarie Windham-Myers, Norman Bliss, Stephen Crooks, James T. Morris, J. Patrick Megonigal, Tiffany Troxler et al. 2018. "Accuracy and precision of tidal wetland soil carbon mapping in the conterminous United States." Scientific reports 8, no. 1: 1-16.

Hopkinson, C. S., Morris, J. T., Fagherazzi, S., Wollheim, W. M., and Raymond, P. A. 2018. Lateral marsh edge erosion as a source of sediments for vertical marsh accretion. Journal of Geophysical Research: Biogeosciences, 123, 2444– 2465. https://doi.org/10.1029/2017JG004358

Howard, J., Hoyt, S., Isensee, K., Pidgeon, E., Telszewski, M. (eds.) 2014. Coastal Blue Carbon: Methods for assessing carbon stocks and emissions factors in mangroves, tidal salt marshes, and seagrass meadows. Conservation International, Intergovernmental Oceanographic Commission of UNESCO, International Union for Conservation of Nature. Arlington, Virginia, USA.

Hill, T. D., and Anisfeld, S. C. 2015. Coastal wetland response to sea level rise in Connecticut and New York. Estuarine, Coastal and Shelf Science, 163(PB), 185–193. https://doi.org/10.1016/J.ECSS.2015.06.004

Howarth, R. W., and Hobbie, J. E. 1982. THE REGULATION OF DECOMPOSITION AND HETEROTROPHIC MICROBIAL ACTIVITY IN SALT MARSH SOILS: A REVIEW. Estuarine Comparisons, 183–207. https://doi.org/10.1016/B978-0-12-404070-0.50017.

IPCC. 2013 Supplement to the 2006 IPCC Guidelines for National Greenhouse Gas Inventories: Wetlands. (IPCC, Switzerland, 2014).

Janousek, C. N., Buffington, K. J., Guntenspergen, G. R., Thorne, K. M., Dugger, B. D., and Takekawa, J. Y. 2017. Inundation, vegetation, and sediment effects on litter decomposition in Pacific Coast tidal marshes. Ecosystems, 20(7), 1296– 1310. https://doi.org/10.1007/s10021-017-0111-6

Kauffman, J. B., Giovanonni, L., Kelly, J., Dunstan, N., Borde, A., Diefenderfer, H., Cornu, C., Janousek, C., Apple, J., and Brophy, L. 2020. Total ecosystem carbon stocks at the marine-terrestrial interface: Blue carbon of the Pacific Northwest Coast, United States. Global Change Biology, 26(10), 5679–5692. https://doi.org/10.1111/GCB.15248.

Kearney, M. S., Rogers, A. S., Townshend, J. R. G., Rizzo, E., Stutzer, D., Stevenson, J. C., and Sundborg, K. 2011. Landsat imagery shows decline of coastal marshes in Chesapeake and Delaware Bays, Eos Trans. AGU, 83(16), 173– 178, https://doi.org/10.1029/2002EO000112.

Kirwan, M. L., & Guntenspergen, G. R. 2010. Influence of tidal range on the stability of coastal marshland. Journal of Geophysical Research: Earth Surface, 115(F2), 2009. https://doi.org/10.1029/2009JF001400

Kirwan, M. L., Guntenspergen, G. R., and Langley, J. A. 2014. Temperature sensitivity of organic-matter decay in tidal marshes. Biogeosciences, 11(17), 4801– 4808. https://doi.org/10.5194/bg-11-4801-2014

Kirwan, M., Temmerman, S., Skeehan, E. et al. 2016. Overestimation of marsh vulnerability to sea level rise. Nature Clim Change 6, 253–260. https://doi.org/10.1038/nclimate2909.

Kroeger, K.D., Crooks, S., Moseman-Valtierra, S. et al. 2017. Restoring tides to reduce methane emissions in impounded wetlands: A new and potent Blue Carbon climate change intervention. Sci Rep 7, 11914. https://doi.org/10.1038/s41598-017-12138-4

Laiho, R. 2006. Decomposition in peatlands: Reconciling seemingly contrasting results on the impacts of lowered water levels. Soil Biology & Biochemistry, 38, 2011– 2024. https://doi.org/10.1016/j.soilbio.2006.02.017

Lalimi, F. Y., Silvestri, S., D'Alpaos, A., Roner, M., and Marani, M. 2018. The Spatial Variability of Organic Matter and Decomposition Processes at the Marsh Scale. Journal of Geophysical Research: Biogeosciences, 123(12), 3713–3727. https://doi.org/10.1029/2017JG004211.

Langley, J. A., McKee, K. L., Cahoon, D. R., Cherry, J. A., and Megonigal, J. P. 2009. Elevated CO2 stimulates marsh elevation gain, counterbalancing sea-level rise. Proceedings of the National Academy of Sciences, 106(15), 6182–6186. https://doi.org/10.1073/PNAS.0807695106.

Lovelock, C. E., Fourqurean, J. W., and Morris, J. T. 2017. Modeled CO2 emissions from coastal wetland transitions to other land uses: Tidal marshes, mangrove forests, and seagrass beds. Frontiers in Marine Science, 4(MAY), 143. https://doi.org/10.3389/FMARS.2017.00143.

Marani, M., D'Alpaos, A., Lanzoni, S., and Santalucia, M. 2011. Understanding and predicting wave erosion of marsh edges. Geophysical Research Letters, 38(21), 21401. https://doi.org/10.1029/2011GL048995.

Mariotti, G., Elsey-Quirk, T., Bruno, G., and Valentine, K. 2020. Mud-associated organic matter and its direct and indirect role in marsh organic matter accumulation and vertical accretion. Limnology and Oceanography, 65(11), 2627-2641.

McLeod, E., Chmura, G. L., Bouillon, S., Salm, R., Björk, M., Duarte, C. M., Lovelock, C. E., Schlesinger, W. H., and Silliman, B. R. 2011. A blueprint for blue carbon: toward an improved understanding of the role of vegetated coastal habitats in sequestering CO2. Frontiers in Ecology and the Environment, 9(10), 552–560. https://doi.org/10.1890/110004.

Moskalski, S. M., and Sommerfield, C. K. 2012. Suspended sediment deposition and trapping efficiency in a Delaware salt marsh. Geomorphology, 139–140, 195–204. https://doi.org/10.1016/J.GEOMORPH.2011.10.018

Morris, J. T., and Bowden, W. B. 1986. A Mechanistic, Numerical Model of Sedimentation, Mineralization, and Decomposition for Marsh Sediments. Soil Science Society of America Journal, 50(1), 96–105. https://doi.org/10.2136/SSSAJ1986.03615995005000010019X.

Morris, J.T., Sundareshwar, P.V., Nietch, C.T., Kjerfve, B. and Cahoon, D.R. 2002. RESPONSES OF COASTAL WETLANDS TO RISING SEA LEVEL. Ecology, 83: 2869-2877. https://doi.org/10.1890/0012-9658(2002)083[2869:ROCWTR]2.0.CO;2.

Morris, J. T., Barber, D. C., Callaway, J. C., Chambers, R., Hagen, S. C., Hopkinson, C. S., Johnson, B. J., Megonigal, P., Neubauer, S. C., Troxler, T., and Wigand, C. 2016. Contributions of organic and inorganic matter to sediment volume and accretion in tidal wetlands at steady state. Earth's future, 4(4), 110–121. https://doi.org/10.1002/2015EF000334.

Mudd, S. M., Howell, S. M., and Morris, J. T. 2009. Impact of dynamic feedbacks between sedimentation, sea-level rise, and biomass production on near-surface marsh stratigraphy and carbon accumulation. Estuarine, Coastal and Shelf Science, 82(3), 377–389. https://doi.org/10.1016/J.ECSS.2009.01.028

Murray, B. C., Pendleton, L., Jenkins, W. A., and Sifleet, S. 2011. Green Payments for Blue Carbon Economic Incentives for Protecting Threatened Coastal Habitats. Nicholas Institute for Environmental Policy Solutions, Duke University Reports.

Nahlik, A. M., and Fennessy, M. S. 2016. Carbon storage in US wetlands. Nature Communications 2016 7:1, 7(1), 1–9. https://doi.org/10.1038/ncomms13835

Neubauer, S. C. 2008. Contributions of mineral and organic components to tidal freshwater marsh accretion. Estuarine, Coastal and Shelf Science, 78(1), 78–88. https://doi.org/10.1016/J.ECSS.2007.11.011

New York State Department of Environmental Conservation (NYSDEC) Lidar: Coastal New York (Long Island and along the Hudson River) from 2010-06-15 to 2010-08-15. NOAA National Centers for Environmental Information, https://www.fisheries.noaa.gov/inport/item/49888.

NOAA: CO-OPS Tidal Datum Calculator. (n.d.). https://access.co-ops.nos.noaa.gov/datumcalc/.

NOAA: Data Access Viewer. (n.d.). https://coast.noaa.gov/dataviewer

NOAA: Tides & Currents - Station Selection. (n.d.). https://tidesandcurrents.noaa.gov/stations.html?type=Datums.

Nyman, J. A., DeLaune, R. D., Roberts, H. H., and Patrick, W. H. 1993. Relationship between vegetation and soil formation in a rapidly submerging coastal marsh. Marine Ecology Progress Series, 96(3), 269–279. http://www.jstor.org/stable/24833555

O'Keefe Suttles, J.A., Eagle, M.J., Mann, A.G., Spivak, A., Sanks, K., Roberts, D., and Kroeger, K.D. 2021. Collection, analysis, and age-dating of sediment cores from natural and restored salt marshes on Cape Cod, Massachusetts, 2015-16: U.S. Geological Survey data release, https://doi.org/10.5066/P9R154DY.

Ouyang, X., and Lee, S.Y. 2020. Improved estimates on global carbon stock and carbon pools in tidal wetlands. Nat Commun 11, 317. https://doi.org/10.1038/s41467-019-14120-2.

Pace, G., Peteet, D., Dunton, M., Wang-Mondaca, C., Ismail, S., Supino, J., and Nichols, J. 2021. Importance of quantifying the full-depth carbon reservoir of Jamaica Bay salt Marshes, New York. City and Environment Interactions, 12, 100073. https://doi.org/10.1016/J.CACINT.2021.100073

Payne, A.R., Burdick, D.M. and Moore, G.E. 2019. Potential Effects of Sea-Level Rise on Salt Marsh Elevation Dynamics in a New Hampshire Estuary. Estuaries and Coasts 42, 1405–1418. https://doi.org/10.1007/s12237-019-00589-z

Pedregosa, F., Varoquaux, Ga"el, Gramfort, A., Michel, V., Thirion, B., Grisel, O., et al. 2011. Scikit-learn: Machine learning in Python. Journal of Machine Learning Research, 12(Oct), 2825–2830.

Pendleton L, Donato DC, Murray BC, Crooks S, Jenkins WA, Sifleet S, et al. 2012. Estimating Global "Blue Carbon" Emissions from Conversion and Degradation of Vegetated Coastal Ecosystems. PLoS ONE 7(9): e43542. https://doi.org/10.1371/journal.pone.0043542

Peteet, D., Nichols, J., Pederson, D., Kenna, T., Chang, C., Newton, B., and Vincent, S. 2020. Climate and anthropogenic controls on blue carbon sequestration in Hudson River tidal marsh, Piermont, New York. Environmental Research Letters, 15(6), 065001. https://doi.org/10.1088/1748-9326/AB7A56.

Peteet, D. M., Nichols, J., Kenna, T., Chang, C., Browne, J., Reza, M., Kovari, S., Liberman, L., and Stern-Protz, S. 2018. Sediment starvation destroys New York City marshes' resistance to sea level rise. Proceedings of the National Academy of Sciences of the United States of America, 115(41), 10281–10286. https://doi.org/10.1073/PNAS.

Raposa, K., Wasson, K., Smith, E., Crooks, J.A., Delgado, P., Fernald, S.H., Ferner, M.C., Helms, A., Hice, L.A., Mora, J.W., Puckett, B, Sanger, D., Shull, S., Spurrier, L., Stevens, R., and Lerberg, S. 2016. Assessing tidal marsh resilience to sea-level rise at broad geographic scales with multi-metric indices. Biol. Conserv., 204, pp. 263-275, https://doi.org/10.1016/j.biocon.2016.10.015

Reed, D. J. 1989. Patterns of sediment deposition in subsiding coastal salt marshes, Terrebonne Bay, Louisiana: The role of winter storms. Estuaries, 12(4), 222– 227. https://doi.org/10.2307/1351901

Reed, D. J. 1995. The response of coastal marshes to sea-level rise: Survival or submergence? Earth Surface Processes and Landforms, 20(1), 39–48. https://doi.org/10.1002/ESP.3290200105

Reed, D. J., Spencer, T., Murray, A. L., French, J. R., and Leonard, L. 1999. Marsh surface sediment deposition and the role of tidal creeks: Implications for created and managed coastal marshes. Journal of Coastal Conservation, 5(1), 81– 90. https://doi.org/10.1007/BF02802742

Rinaldo, A., Fagherazzi, S., Lanzoni, S., Marani, M., and Dietrich, W. E. 1999. Tidal networks 3. Landscape-forming discharges and studies in empirical geomorphic relationships.

Roner, M., Ghinassi, M., Finotello, A., Bertini, A., Combourieu-Nebout, N., Donnici, S., Gilli, A., Vannacci, M., Vigliotti, L., Bellucci, L. G., Fedi, M., Liccioli, L., Tommasini, L., and D'Alpaos, A. 2021. Detecting the Delayed Signatures of Changing Sediment Supply in Salt-Marsh Landscapes: The Case of the Venice Lagoon (Italy). Frontiers in Marine Science, 8, 1477. https://doi.org/10.3389/FMARS.2021.742603/BIBTEX.

Saintilan, N., Wilson, N.C., Rogers, K., Rajkaran, A. and Krauss, K.W. 2014. Mangrove expansion and salt marsh decline at mangrove poleward limits. Glob Change Biol, 20: 147-157. https://doi.org/10.1111/gcb.12341.

Shepard, C. C., Crain, C. M., and Beck, M. W. 2011. The protective role of coastal marshes: a systematic review and meta-analysis. PloS one, 6(11), e27374. https://doi.org/10.1371/journal.pone.0027374

Silliman, B. R., and Bertness, M. D. 2002. A trophic cascade regulates salt marsh primary production. Proceedings of the National Academy of Sciences, 99(16), 10500–10505. https://doi.org/10.1073/PNAS.162366599

Stevens, R., Carter, J., and Peter, C. 2022. An ecological approach to designing salt marshes: Tidal wetland vegetation, elevation, and ecotone boundaries in Great Bay, New Hampshire. https://greatbay.org/wp-content/uploads/2022/03/Designing-Salt-Marshes-March-20221.pdf

Stevens, R. and Shull, S. 2021. Marshes in Context: Exploring marsh resilience at the landscape scale. NOAA & NERRA: Science and Tools for Coastal Communities Nationwide. https://www.nerra.org/wp-content/uploads/2021/11/Broport_11_7-1.pdf.

Temmerman, S., Bouma, T. J., Govers, G., Wang, Z. B., Vries, M. B. De, and Herman, P. M. J. 2005. Impact of vegetation on flow routing and sedimentation patterns: Three-dimensional modeling for a tidal marsh. Journal of Geophysical Research: Earth Surface, 110(F4), 4019. https://doi.org/10.1029/2005JF000301

Temmerman, S., Govers, G., Wartel, S., and Meire, P. 2003. Spatial and temporal factors controlling short-term sedimentation in a salt and freshwater tidal marsh, Scheldt estuary, Belgium, SW Netherlands. Earth Surface Processes and Landforms, 28(7), 739–755. https://doi.org/10.1002/ESP.495

Temmerman, S., Bouma, T. J., Govers, G., and Lauwaet, D. 2005. Flow Paths of Water and Sediment in a Tidal Marsh: Relations with Marsh Developmental Stage and Tidal Inundation Height. Estuarine Research Federation Estuaries, 28(3), 338–352. www.ecnc.nl.

Turner, R. E., Baustian, J. J., Swenson, E. M., and Spicer, J. S. 2006. Wetland sedimentation from hurricanes Katrina and Rita. Science, 314(5798), 449– 452. https://doi.org/10.1126/science.1129116

Twilley, R. R., Rovai, A. S., and Riul, P. 2018. Coastal morphology explains global blue carbon distributions. Frontiers in Ecology and the Environment, 16(9), 503–508. https://doi.org/10.1002/FEE.1937.

Ursino, N., Silvestri, S., and Marani, M. 2004. Subsurface flow and vegetation patterns in tidal environments, Water Resour. Res., 40, W05115, doi:10.1029/2003WR002702.

U.S. Department of Agriculture Natural Resources Conservation Service. 2008. Soil Quality Indicators: Bulk Density https://cafnr.missouri.edu/wp-content/uploads/2016/09/bulk-density.pdf

U.S. Department of Commerce, N.G.S. (n.d.). National Spatial Reference System, Geodetic control map. https://geodesy.noaa.gov/NGSDataExplorer/

U.S. Fish & Wildlife Service. 2018. National Wetlands Inventory. U.S. Fish & Wildlife Service. https://data.nal.usda.gov/dataset/national-wetlands-inventory.

U.S. Geological Survey CMGP LiDAR: Post Sandy (MA, NH, RI) from 2010-06-15 to 2010-08-15. NOAA National Centers for Environmental Information, https://www.fisheries.noaa.gov/inport/item/49846.

Valiela, I., Teal, J. M., Allen, S. D., Vanetten, R., Goehringer, D., and Volkmann, S. 1985. Decomposition in salt-marsh ecosystems—The phases and major factors affecting disappearance of above-ground organic-matter. Journal of Experimental Marine Biology and Ecology, 89(1), 29– 54. https://doi.org/10.1016/0022-0981(85)90080-2

van Ardenne, L. B. van, Jolicouer, S., Bérubé, D., Burdick, D., and Chmura, G. L. 2018. The importance of geomorphic context for estimating the carbon stock of salt marshes. Geoderma, 264–275. https://doi.org/10.1016/J.GEODERMA.2018.06.003.

van de Broek, M., Temmerman, S., Merckx, R. and Govers, G. 2016. The importance of an estuarine salinity gradient on soil organic carbon stocks of tidal marshes. https://doi.org/10.5194/bg-2016-285.

van Proosdij, D., Davidson-Arnott, R. G. D., and Ollerhead, J. 2006. Controls on spatial patterns of sediment deposition across a macro-tidal salt marsh surface over single tidal cycles. Estuarine, Coastal and Shelf Science, 69(1–2), 64–86. https://doi.org/10.1016/J.ECSS.2006.04.022.

Vinent, O. D., Herbert, E. R., Coleman, D. J., Himmelstein, J. D., and Kirwan Correspondence, M. L. 2021. Onset of runaway fragmentation of salt marshes. https://doi.org/10.1016/j.oneear.2021.02.013.

Wang, F, Kroeger, KD, Gonneea, ME, Pohlman, JW, and Tang, J. 2019. Water salinity and inundation control soil carbon decomposition during salt marsh restoration: An incubation experiment. Ecol Evol.; 9: 1911– 1921. https://doi.org/10.1002/ece3.4884

Watson, E.B., Wigand, C., Davey, E.W. et al. 2017. Wetland Loss Patterns and Inundation-Productivity Relationships Prognosticate Widespread Salt Marsh Loss for Southern New England. Estuaries and Coasts 40, 662–681. https://doi.org/10.1007/s12237-016-0069-1

Weston, N.B., Neubauer, S.C., Velinsky, D.J. et al. 2014. Net ecosystem carbon exchange and the greenhouse gas balance of tidal marshes along an estuarine salinity gradient. Biogeochemistry 120, 163–189. https://doi.org/10.1007/s10533-014-9989-7.

Wilson, C.A., Z.J. Hughes, D.M. FitzGerald, C.S. Hopkinson, V. Valentine, and A.S. Kolker. 2014. Saltmarsh pool and tidal creek morphodynamics: Dynamic equilibrium of northern latitude saltmarshes? Geomorphology 213: 99–115. https://doi.org/10.1016/j.geomorph.2014.01.002.

Yang, H., Tang, J., Zhang, C., Dai, Y., Zhou, C., Xu, P., et al. 2020. Enhanced carbon uptake and reduced methane emissions in a newly restored wetland. Journal of Geophysical Research: Biogeosciences, 125, e2019JG005222. https://doi.org/10.1029/2019JG005222

Zeff, M. L. 1988. Sedimentation in a salt marsh-tidal channel system, southern New Jersey. Marine Geology, 82(1–2), 33–48. https://doi.org/10.1016/0025-3227(88)90005-9